

The ORP9-ORP11 dimer promotes sphingomyelin synthesis

Reviewed Preprint

v2 • July 25, 2024


Revised by authors

Reviewed Preprint

v1 • September 29, 2023

Birol Cabukusta ✉, Shalom Borst Pauwels, Jimmy J.L.L. Akkermans, Niek Blomberg, Aat A. Mulder, Roman I. Koning, Martin Giera, Jacques Neefjes

Cell and Chemical Biology, Oncode Institute, Leiden University Medical Center, Leiden, Netherlands • Centre for Proteomics and Metabolomics, Leiden University Medical Center, Leiden, Netherlands • Electron Microscopy Facility, Cell and Chemical Biology, Leiden University Medical Center, Leiden, Netherlands

 https://en.wikipedia.org/wiki/Open_access Copyright information

Abstract

Numerous lipids are heterogeneously distributed among organelles. Most lipid trafficking between organelles is achieved by a group of lipid transfer proteins (LTPs) that carry lipids using their hydrophobic cavities. The human genome encodes many intracellular LTPs responsible for lipid trafficking and the function of many LTPs in defining cellular lipid levels and distributions is unclear. Here, we created a gene knockout library targeting 90 intracellular LTPs and performed whole-cell lipidomics analysis. This analysis confirmed known lipid disturbances and identified new ones caused by loss of LTPs. Among these, we found major sphingolipid imbalances in ORP9 and ORP11 knockout cells, two proteins of previously unknown function in sphingolipid metabolism. ORP9 and ORP11 form a heterodimer to localize at the ER-*trans* Golgi membrane contact sites, where the dimer exchanges phosphatidylserine (PS) for phosphatidylinositol-4-phosphate (PI(4)P) between the two organelles. Consequently, loss of either protein causes phospholipid imbalances in the Golgi apparatus that result in lowered sphingomyelin synthesis at this organelle. Overall, our LTP knockout library toolbox identifies various proteins in control of cellular lipid levels, including the ORP9-ORP11 heterodimer, which exchanges PS and PI(4)P at the ER-Golgi membrane contact site as a critical step in sphingomyelin synthesis in the Golgi apparatus.

eLife assessment

This **valuable** manuscript systematically addresses the role of intracellular lipid transfer proteins on cellular lipid levels. It provides **convincing** evidence on the role of ORP9 and ORP11 in sphingolipid metabolism at the Golgi complex. This article will be of broad interest to cell biologists interested in lipid metabolism and membrane biology.

<https://doi.org/10.7554/eLife.91345.2.sa3>

Introduction

Many types of lipids are heterogeneously distributed among various organelles of the cell¹. Due to the hydrophobic nature of lipids, their trafficking needs to be facilitated. While vesicular trafficking transports lipids in bulk between organelles, non-vesicular trafficking of lipids also play a role in defining lipid compositions of organelles. In fact, many organelles that do not receive any vesicular cargo rely on this route. Non-vesicular trafficking of lipids is achieved by a group of lipid transfer proteins (LTPs) that carry lipids using their hydrophobic cavities to stabilize lipids in the aqueous intracellular environment². LTPs often contain targeting domains, motifs, transmembrane regions, amphipathic helices or surface charge to define their donor and acceptor organelles³. Many LTPs localize at two organelles simultaneously at membrane contact sites, where these organelles come closer to exchange information and material, including lipids^{4,5}.

The human genome encodes over 150 LTPs; new LTPs and LTP families are being characterized every so often^{2,6-13}. About 50 of these proteins are secreted and are involved in carrying lipids, metals, lipopolysaccharides, and other small molecules in blood plasma². The remaining intracellular LTPs are mainly responsible for intracellular lipid trafficking among organelles. Since many lipid-modifying enzymes are localized to different organelles, LTPs also feed metabolic lipid fluxes, eventually defining cellular lipid levels¹⁴. For example, LTP-mediated trafficking of ceramide from the endoplasmic reticulum (ER) to the *trans* Golgi is needed for sphingomyelin synthesis¹⁵. While achieving a considerable understanding of some LTPs in the last years, the function of many LTPs in defining cellular levels and distributions remains unclear.

To study LTPs systematically, we designed and created an arrayed gene knockout library targeting 90 intracellular LTPs based on the CRISPR/Cas9 technology. Lipidomics analysis of the library-generated LTP knockout cells confirmed known and identified novel lipid disturbances emerging from loss of LTPs. These included CERT, GLTP, NPC1 and NPC2 knockout cells with altered sphingolipid levels. Furthermore, we identified major sphingolipid imbalances in ORP9 and ORP11 knockout cells, two proteins of unknown function in sphingolipid metabolism. ORP9 and ORP11 form a heterodimer to localize at the ER-*trans* Golgi membrane contact sites. At this contact site, the ORP9-ORP11 dimer transfers phosphatidylserine (PS) from the ER to the Golgi and phosphatidylinositol-4-phosphate (PI(4)P) in the opposite direction. Consequently, loss of either protein causes phospholipid imbalances in the Golgi apparatus that results in lowered sphingomyelin synthesis capacity at this organelle. Collectively, our LTP knockout library toolbox identified various proteins controlling cellular lipid levels. Among these, we found the ORP9-ORP11 heterodimer defining phospholipid composition of the *trans* Golgi as a critical step in sphingomyelin synthesis. These findings highlighted that phospholipid and sphingolipid gradients along the secretory pathway are linked at the ER-Golgi membrane contact sites.

Results

1) A CRISPR knockout library targeting lipid transfer proteins

To understand the function of LTPs in defining cellular levels and distributions, we created an arrayed CRISPR/Cas9 knockout library targeting LTPs. We targeted only the intracellular LTPs in the library and excluded extracellular proteins, such as LIPOCALIN and LBP-BPI-CETP families². In this library, 90 wells of a 96-well plate were used for targeting LTPs and 6 for non-targeting (NT) controls (Fig. 1A). For optimal gene disruption, we used a lentiviral gene delivery system and 3

guide RNAs per gene – a method also used by others to increase the frequency of gene disruption¹⁶. We applied the LTP knockout library to MelJuSo, a human melanoma cell line. The efficiency of the knockout strategy was confirmed by western blotting of selected wells (**Fig. 1B**).

Next, we performed whole-cell lipidomics analysis of the LTP knockout cells. To this end, library-generated MelJuSo cells were grown in lipid-depleted serum and analysed using a lipidomics platform detecting 17 different lipid classes thrice on average (**Fig. 1A**). One of the detected lipid classes, hexosylceramide, can correspond to glucosylceramide and galactosylceramide – two isomeric lipids in mammalian cells. By metabolic chasing of a fluorescent ceramide analogue in cells silenced for glucosylceramide synthase or galactosylceramide synthase; or treated with the glucosylceramide synthase inhibitor PDMP, we validated that glucosylceramide is the major hexosylceramide in MelJuSo cells (Fig. S1). This further substantiated the previous reports of galactosylceramide being present mainly in oligodendrocytes¹⁷.

We next calculated the z-scores within each lipid class based on their relative abundance per measurement and plotted their average for LTP knockout cell lines. The analysis revealed many LTP knockout cells with lipid imbalances (**Fig. 1C**, Fig. S2A). Meanwhile, no z-score above the absolute value of 2 was observed for NT control cells (Fig. S2B). Overall, the lipidomics analysis of the LTP knockout library uncovered numerous candidate regulators of cellular lipid levels.

2) NPC1 and NPC2 knockout cells accumulate sphingomyelin in lysosomes and the plasma membrane

Lipidomics analysis of the LTP knockout library revealed various anticipated imbalances. Among these candidate regulators of cellular lipid levels, those related to sphingolipid metabolism are notable. This is likely due to many enzymatic steps of sphingolipid metabolism being more linear and lacking the elasticity of phospholipids¹⁴. In the analysis, we identified GLTP knockout cells with lowered glucosylceramide levels (**Fig. 2A**, Fig. S3A-C). Loss of GLTP is recently reported to block ER-to-Golgi anterograde vesicular trafficking that results in lowered glucosylceramide synthesis¹⁸.

In addition, we observed NPC1 and NPC2 knockout cells with elevated sphingolipid levels (**Fig. 1B**). Mutations in *NPC1* and *NPC2* genes are the cause of Niemann-Pick disease, type C that leads to lysosomal accumulation of cholesterol¹⁹. Cells lacking NPC1 or NPC2 function also accumulate sphingolipids²⁰. Our observation of elevated sphingolipid levels in NPC1 and NPC2 knockout cells was present in all sphingolipid classes (**Fig. 2B, C**). Meanwhile phospholipid levels were not altered dramatically in these cells (Fig. S3D). To confirm whether this increase is associated with lysosomal accumulation of sphingolipids, we used a sphingomyelin-binding biosensor based on the equinatoxin secreted by the beadlet anemone *Actinia equina* (Fig. S3E)^{21,22}. Immunofluorescence staining of NPC1 and NPC2 knockout cells using the biosensor showed lysosomal accumulation of sphingomyelin (**Fig. 2D**). Flow cytometry analysis using the sphingomyelin biosensor and the GM1 glycosphingolipid biosensor, the B subunit of cholera toxin, demonstrated that sphingolipid accumulation is also reflected on the cell surface of NPC1 and NPC2 knockouts (**Fig. 2E, F**). Meanwhile, the surface protein levels were not altered as detected by staining for the tetraspanin protein CD63. Collectively, our results corroborate the sphingolipid accumulation in NPC1 and NPC2 deficient cells and illustrate that the LTP knockout library is a viable tool to study LTPs and their role in regulating cellular lipid levels.

3) CERT, ORP9 and ORP11 knockout cells demonstrate reduced sphingomyelin levels

Sphingomyelin is the major sphingolipid in mammalian cells, and it is mainly synthesized in the *trans* Golgi from ceramide delivered from the ER. The non-vesicular trafficking of ceramide from the ER to the *trans* Golgi is mediated by the ceramide transfer protein CERT^{15,23} (**Fig. 3B**).

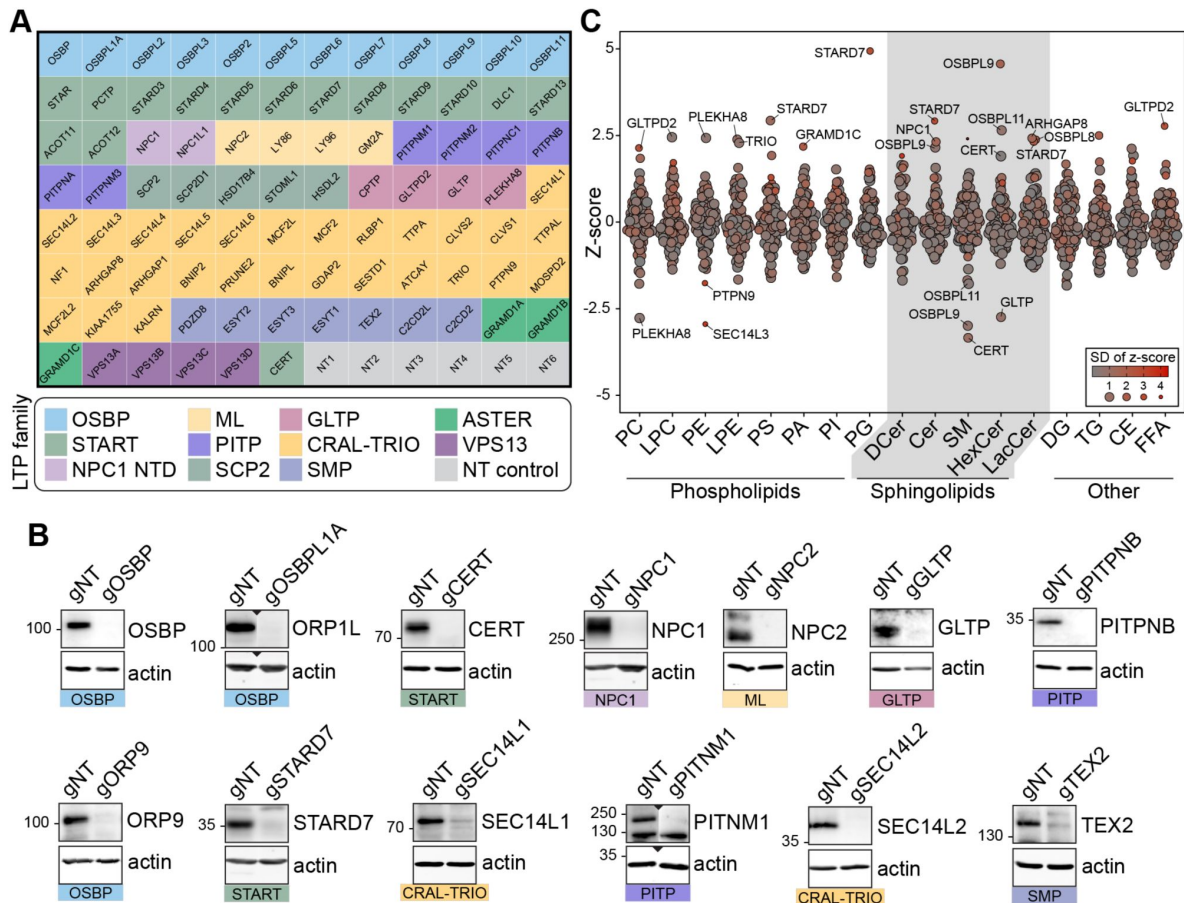


Figure 1

Lipidomics analysis of a LTP knockout library revealed known and candidate controllers of cellular lipid levels.

(A) Overview of the arrayed gene knockout library targeting LTPs. NT: non-targeting. (B) Western blotting of the selected wells showing the efficiency of the LTP knockout library on MelJuSo cells. gNT: Non-targeting, control cells. (C) Summary plot of the lipidomics analysis: Z-scores calculated for 17 lipid classes are plotted. Each data point represents the mean Z-score of an LTP knockout cell line; size and color of data points represent the standard deviation of Z-scores for 3 experiments on average. PC: phosphatidylcholine, LPC: lyso-phosphatidylcholine, PE: phosphatidylethanolamine, LPE: lyso-phosphatidylethanolamine, PS: phosphatidylserine, PI: phosphatidylinositol, PA: phosphatidic acid, PG: phosphatidylglycerol, DCer: dihydroxyceramide, Cer: ceramide, SM: sphingomyelin, HexCer: hexosylceramide, LacCer: lactosylceramide, DG: diacylglycerol, TG: triacylglycerol, CE: cholesterol ester, FFA: free fatty acids.

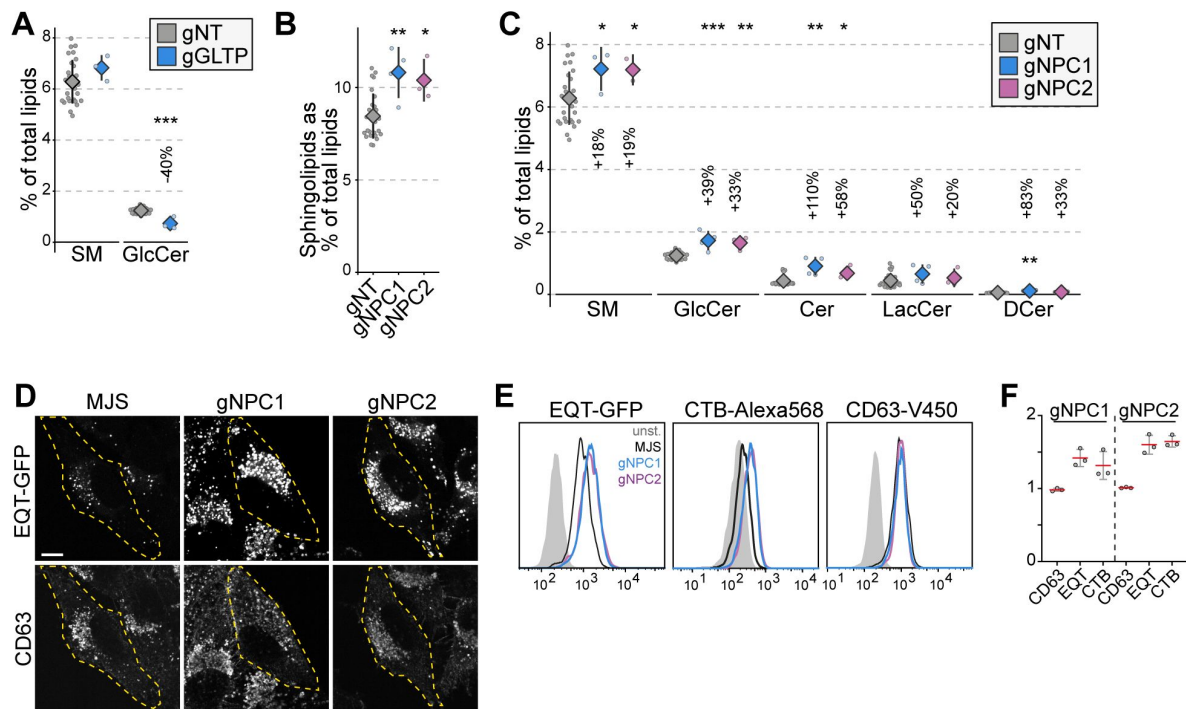


Figure 2

NPC1 and NPC2 knockout cells accumulate sphingomyelin in lysosomes.

(A) GLTP knockouts show decreased glucosylceramide levels compared to control cells. GlcCer: glucosylceramide (B) NPC1 and NPC2 knockout cells have increased sphingolipids levels compared to control cells. (C) Increased sphingolipid levels in NPC1 and NPC2 knockouts are represented in all sphingolipid classes. (D) Immunofluorescence images of NPC1 and NPC2 knockout cells permeabilized and stained with recombinant GFP-EQT show the accumulation of sphingomyelin in the lysosomes compared to the parental MelJuSo (MJS) cells. Pixel intensities of the images were adjusted evenly. Scale bar 10µm. (E) Flow cytometry analysis of cells stained with EQT-GFP, CTB-Alexa568 and CD63-V450 on the cell surface. Analysis demonstrates the accumulation of sphingomyelin (EQT-GFP) and the glycosphingolipid GM1 (CTB-Alexa568) on the cell surface without affecting the surface protein levels. (F) Mean fluorescence intensities for each staining normalized to control cells from 3 experiments. Red lines and error bars correspond to mean and standard deviations from 3 experiments, respectively. Approximately 2000 cells were analyzed per experiment.

Our analysis identified CERT knockouts with the lowest sphingomyelin levels (**Fig. 1C** [↗](#), 3A). These cells also demonstrate increased glucosylceramide levels, likely as a compensation mechanism (**Fig. 3A** [↗](#)). Furthermore, we found decreased sphingomyelin and increased glucosylceramide levels in ORP9 and ORP11 knockout cells – two proteins of unknown role in sphingolipid metabolism (**Fig. 1C** [↗](#), 3A). The sphingolipid imbalances in all three knockout cells – CERT, ORP9, and ORP11 – were also represented in many sphingolipid subspecies (**Fig. 3C** [↗](#), Fig. S4B). Lowered sphingomyelin levels of the three knockout cells were further confirmed by their sensitivity towards methyl- β -cyclodextrin treatment (**Fig. 3D** [↗](#)). Meanwhile, none of the three knockout cells demonstrated phospholipid imbalances to a compelling degree (Fig. S4A).

The observation that ORP9 and ORP11 knockout cells mimic CERT knockouts implied a role for ORP9 and ORP11 in *de novo* sphingomyelin synthesis, whereas loss of neither ORP9 nor ORP11 reduced CERT protein levels (**Fig. 3E** [↗](#)). ORP9 and ORP11 each contain a PH domain mediating localization at the *trans* Golgi, the site of *de novo* sphingomyelin synthesis (**Fig. 3F** [↗](#), G). As loss of either ORP9 or ORP11 did not alter the Golgi ultrastructure as detected by light or electron microscopy (Fig. S5), it further suggested that ORP9 and ORP11 affect sphingomyelin levels by a previously unknown mechanism. Next, we investigated the possible mechanism by which ORP9 and ORP11 regulate cellular sphingolipid levels.

4) Dimerization is critical for the ER-Golgi contact site localization of ORP9 and ORP11

ORP9 and ORP11 interact with each other via their regions between their PH and ORD domains²⁴ [↗](#). As no other domain is found in this region, we speculated some secondary structures must facilitate the dimerization. AlphaFold and PCOILS coiled coils prediction tool suggested that ORP9 and ORP11 contain two alpha helices each in this region – hereafter referred as “coils” (**Fig. 4A, S6A, B** [↗](#)). AlphaFold-Multimer suggested that the coils of ORP9 and ORP11 interact with each other (**Fig. 4B** [↗](#), S6C-D). Identical analysis of the full-length proteins predicted that the coils drive dimerization of the two proteins (**Fig. 4C, D, S6E** [↗](#)). This was tested by targeting the coils of ORP9 to the mitochondrial outer membrane using the *N*-terminal sequence of TOM70. In cells expressing mitochondria-targeted ORP9 coils, the coils of ORP11 located to this organelle (**Fig. 4C, D** [↗](#)). The absence of either coil prevented the colocalization, suggesting that the coils of ORP9 and ORP11 are sufficient for their dimerization. This finding was validated by co-immunoprecipitations (**Fig. 4E** [↗](#)).

ORP9, but not ORP11, contains a FFAT, two phenylalanines in an acidic tract, motif that drives ER localization by interacting with the ER-resident VAPA and VAPB²⁵ [↗](#). Despite not containing a FFAT motif, ORP11 could interact with VAPA and VAPB by its dimerization with ORP9. We tested this by co-immunoprecipitations, where ORP11 could be co-isolated with VAPA from cells expressing VAPA, ORP9 and ORP11 (**Fig. 4J** [↗](#)). This interaction was diminished significantly when ORP9 was not co-expressed. Furthermore, a VAPA mutant unable to interact with FFAT motifs failed to interact with either ORP9 or ORP11, showing that ORP11 interacts with VAPA indirectly via the ORP9-FFAT motif.

We and others previously showed that in addition to VAPA and VAPB, the human proteome contains three other proteins interacting with FFAT and related short linear motifs: MOSPD1, MOSPD2 and MOSPD3²⁶ [↗](#),²⁷ [↗](#). In our earlier efforts to identify interaction partners of VAPA, VAPB and other motif-binding proteins, we performed BioID, proximity biotinylation followed by proteomics, identification of membrane contact sites proteins²⁷ [↗](#). In this analysis, ORP9 and ORP11 were found in proximity with VAPA and VAPB but not with other motif-binding proteins (Fig. S6F). This further confirmed that despite lacking a FFAT motif, ORP11 together with ORP9 is part of VAPA- and VAPB-mediated membrane contact sites.

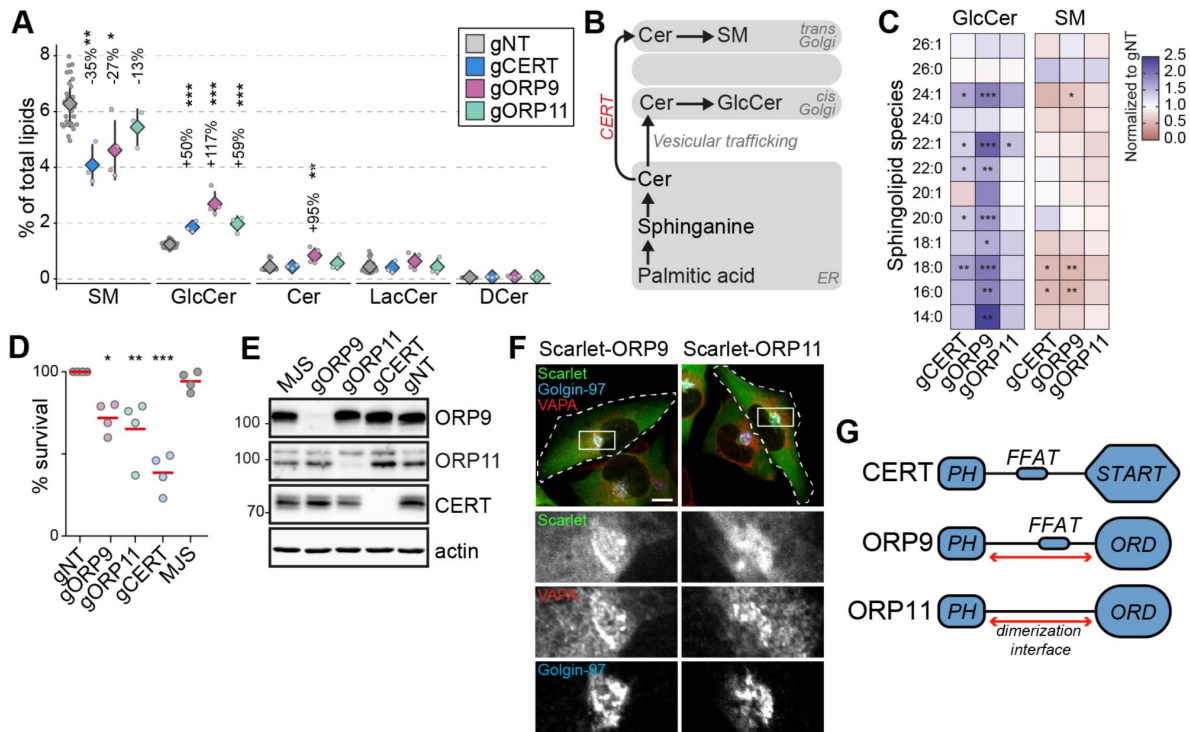


Figure 3

CERT, ORP9 and ORP11 knockout cells demonstrate reduced sphingomyelin levels.

(A) CERT, ORP9 and ORP11 knockouts demonstrate decreased sphingomyelin and increased glucosylceramide levels. (B) Schematic representation of *de novo* sphingomyelin synthesis pathway of mammalian cells. (C) Decreased sphingomyelin and increased glucosylceramide levels observed in knockout cells are present in various sphingolipid subspecies. (D) Similar to CERT knockouts, ORP9 and ORP11 knockouts are sensitive to methyl- β -cyclodextrin treatment. Red lines correspond to mean values from 4 experiments. (E) Western blot of knockout cells showing that the loss of ORP9 or ORP11 does not affect CERT protein levels. (F) ORP9 and ORP11 localize at the Golgi apparatus. Scale bar 10 μ m. (G) Domain architecture of CERT, ORP9 and ORP11. All proteins contain PH domains for Golgi localization. CERT and ORP9, but not ORP11, contain a FFAT motif for interacting with VAP proteins.

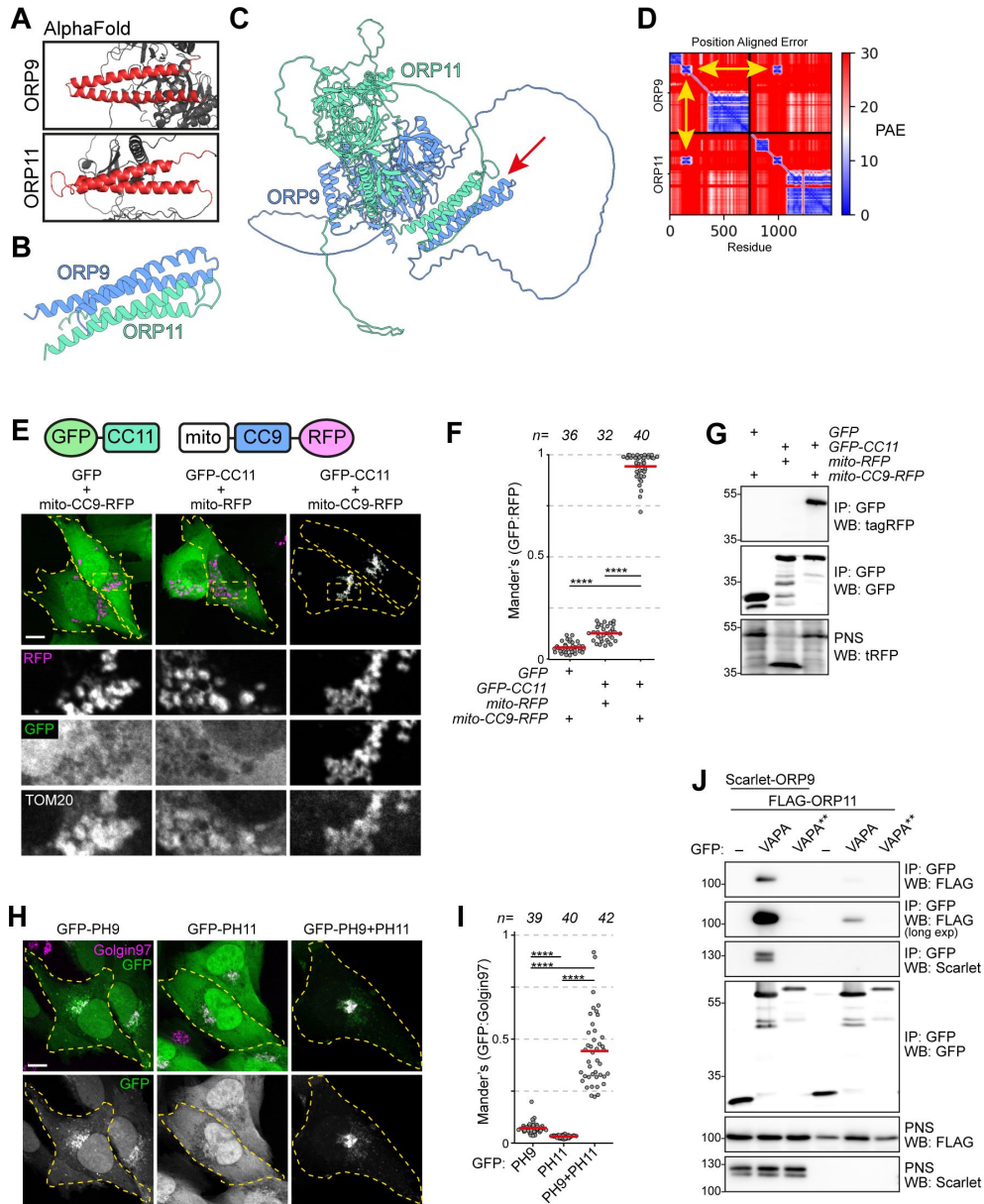


Figure 4

ORP9 dimerization is critical for ER localization of ORP11.

(A) AlphaFold revealing coiled coils in ORP9 and ORP11. (B) AlphaFold-Multimer shows that coiled coils of ORP9 and ORP11 interacting with each other. (C) ColabFold protein complex prediction for full length ORP9 and ORP11 shows the dimerization via coiled coils (arrow). (D) Position aligned error for panel C. Note that the interaction of coils has a lower score (yellow arrows). (E) Coiled coils of ORP9 and ORP11 is sufficient to define their localization as ORP11 coiled coils colocalizes with the mitochondria-targeted ORP9 coiled coils at mitochondria. Scale bar: 10µm. (F) Colocalization analysis of immunofluorescent images corresponding to panel E. Red lines correspond to mean values from 3 experiments; n is number of analyzed cells. (G) Co-immunoprecipitation confirming that the coils of ORP9 and ORP11 interact with each other. (H) Immunofluorescence images of PH domain localizations. Compared to individual PH domains of ORP9 and ORP11, ORP9-ORP11 chimera demonstrates better affinity towards the Golgi. Scale bar: 10µm. (I) Colocalization analysis of immunofluorescent images corresponding to panel H. Red lines correspond to mean values from 3 experiments; n is number of analyzed cells. (J) Co-immunoprecipitation analysis of VAPA, ORP9 and ORP11 from over-expressing cells. Despite lacking a FFAT motif, ORP11 interacts with the ER-resident VAPA protein. This interaction is facilitated by the FFAT motif of ORP9 as a VAPA mutant unable to interact with FFAT motifs (VAPA**) was unable to co-precipitate ORP9 or ORP11.

The Golgi localization of ORP9 and ORP11 is mediated by their PH domain interacting with phosphatidylinositol phosphates²⁴. We observed that the PH domains of ORP9 and ORP11 localized only partially to the Golgi and demonstrated strong cytoplasmic localization, unlike the PH domains of OSBP and CERT that show exclusive localization to this organelle^{28,29} (Fig. 4H, I, S7D). We hypothesized that the dimerization of ORP9 and ORP11 is a mechanism to increase their avidity towards *trans* Golgi membranes. To test this, we created a chimera containing ORP9- and ORP11-PH domains that localized to the Golgi more efficiently than the individual PH domains (Fig. 4H, I). This also implied that loss of either protein should reduce the other's localization to the *trans* Golgi. Immunofluorescence staining of ORP9 and ORP11 knockout cells for the same proteins confirmed that both ORP9 and ORP11 are required for the Golgi localization of the other protein (Fig. 5). Meanwhile, loss of either protein did not influence the levels of the other (Fig. 3E). Our results collectively show that the dimerization of ORP9 and ORP11 via their coils is required for the localization of ORP9-ORP11 dimer to the ER and the *trans* Golgi simultaneously.

5) ORP9 and ORP11 are essential for PS and PI(4)P levels in the Golgi apparatus

ORP9 and ORP11 belong to the OSBP-related protein (ORP) family that transfers sterols or PS while transferring phosphatidylinositol phosphates in the opposite direction³⁰⁻³³ (Fig. 6A, S7B). ORP9 and ORP11 carry the conserved PS binding site and are recently shown to relocate to the site of lysosomal damage to supply PS for membrane repair³⁴. Using an *in vitro* lipid transfer assay, we confirmed that the lipid transfer domains (ORD) of ORP9 and ORP11 are sufficient to traffic PS *in vitro* (Fig. 6B, C). ORP9 and ORP10, but not ORP11, are shown to traffic PI(4)P^{35,36}. Using a PI(4)P transfer assay that utilizes the PI(4)P-binding PH domain of FAPP1, we show that ORD of ORP11 can also traffic PI(4)P between model membranes (Fig. 6D, E, S7C, D)³⁷. Furthermore, similar to ORP5, ORP8 and ORP10, the PS-trafficking activity of ORP9- and ORP11-ORDs was improved when acceptor liposomes were decorated with PI(4)P^{35,38,39} (Fig. S7E). This indicated that ORDs of ORP9 and ORP11 transport PI(4)P in the opposite direction of PS trafficking.

To demonstrate the contribution of ORP9-ORP11 dimerization to their lipid transfer ability at membrane contact sites, we reconstituted these sites *in vitro* by attaching a His-tagged VAPB devoid of its transmembrane helix to donor liposomes and providing full-length ORP9 and ORP11 as tethers to the acceptor liposomes (Fig. 6F, S7F-H). PS transfer assay in these reconstituted contact sites showed that as a trimer, the ORP9-ORP11-VAPB complex displays an improved lipid transfer capacity (Fig. 6G, H).

PS is synthesized in the ER and its concentration increases along the secretory pathway as it is enriched on the cytosolic leaflet of the plasma membrane¹⁴. PI(4)P, on the other hand, is abundant in the *trans* Golgi, where it recruits many proteins to this membrane⁴⁰. Another LTP localized at the ER-*trans* Golgi membrane contact sites, OSBP transfers cholesterol from the ER to the *trans* Golgi, while counter transporting PI(4)P to the ER for its hydrolysis by the ER-resident PI(4)P phosphatase SAC1 (Fig. 8). Homologous to OSBP, the ORP9-ORP11 dimer resides in the ideal intracellular interface to traffic PS in anterograde and PI(4)P in retrograde direction between the ER and *trans* Golgi (Fig. 8). This also suggested that the loss of either protein would cause PS and PI(4)P imbalances between the ER and *trans* Golgi. We tested this notion by using PI(4)P- and PS-binding biosensors^{41,42} (Fig. S7I, J). Golgi localization of these sensors indicated that PS levels were decreased in the Golgi of these cells (Fig. 6I, J). Also, PI(4)P showed accumulation in the Golgi of ORP9 and ORP11 knockout cells (Fig. 6K, L). We confirmed the PI(4)P accumulation by quantifying the Golgi localization of a PI(4)P specific antibody (Fig. S7J). Interestingly, both phenotypes, lowered PS and increased PI(4)P levels, were better pronounced in ORP9 knockout cells compared to ORP11 knockouts. Furthermore, both phenotypes could be rescued by reconstitution of the missing protein (Fig. 6J, L). Overall, these findings suggested that the ORP9-ORP11 dimer is required for maintaining PS and reducing PI(4)P levels in the Golgi apparatus.

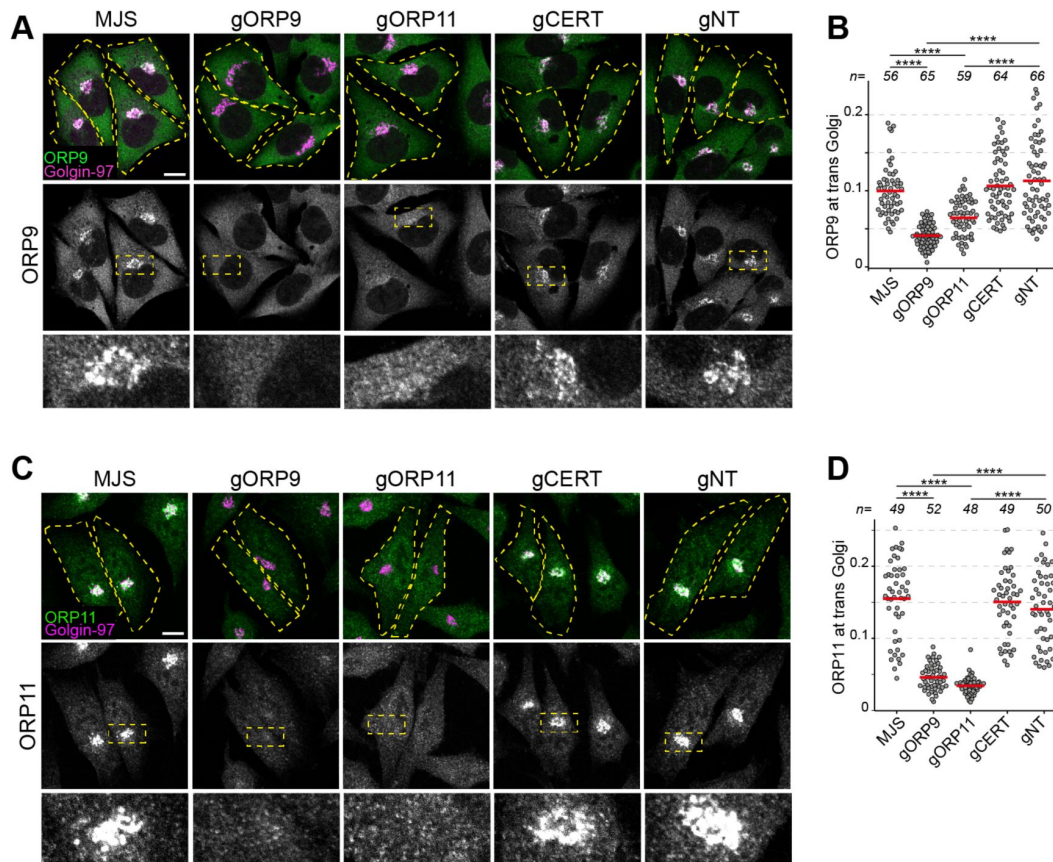


Figure 5

ORP9 and ORP11 dimerization is critical for their Golgi localization.

(A) Immunofluorescence images of cells stained for ORP9. ORP9 fails to localize at the Golgi as efficiently in ORP11 knockout cells. (B) Colocalization analysis of immunofluorescent images corresponding to panel A. Red lines correspond to mean values from 3 experiments; n is number of analyzed cells. (C) Immunofluorescence images of cells stained using an ORP11 antibody. Similar to ORP9, ORP11 fails to localize at the Golgi as efficiently in ORP9 knockout cells. Note that the effect of ORP9 loss on ORP11 localization is more dramatic than vice versa. (D) Colocalization analysis of immunofluorescent images from panel C. Red lines correspond to mean values from 3 experiments; n is number of analyzed cells. All scale bars are 10µm.

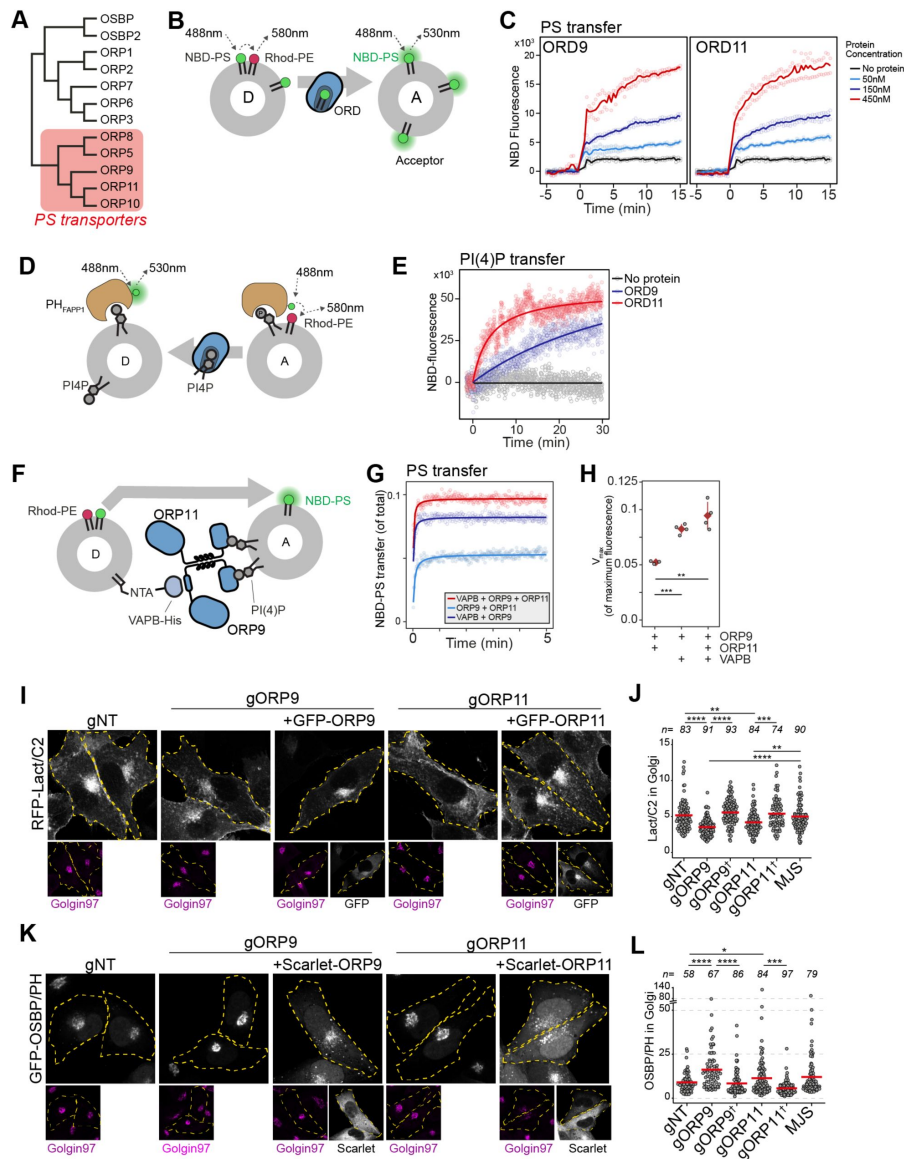


Figure 6

ORP9 and ORP11 are essential for PS and PI(4)P levels in the Golgi apparatus.

(A) Phylogenetic tree of human OSBP-related domains showing that ORP9 and ORP11 belong to the PS transporter branch. (B) Schematic representation of FRET-based PS transfer assay. Rhodamine in the donor vesicles quenches NBD fluorescence unless NBD-labeled lipid is transferred to acceptor liposomes. (C) FRET-based lipid transfer assay using the OSBP-related domains of ORP9 and ORP11, ORD9 and ORD11 respectively, demonstrate the PS trafficking ability between vesicles *in vitro*. (D) Graphical representation of PI(4)P transfer assay that utilizes the NBD-labelled PH domain of FAPP1. PI(4)P transfer by a protein leads to increase NBD-fluorescence by dequenching. (E) PI(4)P transfer assay using ORP9-ORD and ORP11-ORD (ORD9 and ORD11, respectively). (F) Schematic representation of *in vitro* reconstitution of membrane contact sites for lipid transfer assays. (G) PS transfer assay at *in vitro* reconstituted membrane contact sites formed by the VAPB-ORP9-ORP11 trimer. (H) V_{max} quantifications of PS transfer assays from panel E. (I) The PS sensor Lact-C2 localizes less prominently to the Golgi in ORP9 and ORP11 knockout cells. (J) Golgi quantification of the PS sensor RFP-LactC2 indicates reduced PS levels in this organelle. This phenotype could be rescued by reconstitution of the missing protein in knockout cells (shown with a dagger). Red lines correspond to mean values from 3 experiments; n is number of analyzed cells. (K) The PI(4)P sensor OSBP- PH localizes more prominently to the Golgi area in ORP9 and ORP11 knockout cells. (L) Golgi quantification of the PI(4)P sensor confirms the accumulation of PI(4)P at this organelle. This phenotype was rescued by reconstitution of the missing protein in knockout cells (shown with a dagger). Red lines correspond to mean values from 3 experiments; n is number of analyzed cells.

6) *De novo* sphingomyelin synthesis in the Golgi is impaired in ORP9 and ORP11 knockouts

Next, we set out to investigate the possible role of ORP9 and ORP11 in regulating cellular sphingomyelin levels. By performing a sphingomyelin synthase activity assay that uses the fluorescent ceramide analogue NBD-ceramide as a substrate⁴³, we found that ORP9 and ORP11 knockout cells do not have reduced sphingomyelin synthesis capacity (**Fig. 7A, B**). The same was also found in CERT knockout cells. Whereas all three knockouts demonstrated increased glucosylceramide synthesis capacity, supporting the lipidomics analysis (**Fig. 3A**). Unaltered sphingomyelin synthesis capacity was further validated by the unreduced protein and mRNA levels of both human sphingomyelin synthases, SMS1 and SMS2 (**Fig. S8A, B**).

SMS1 is localized at the *trans* Golgi, while SMS2 mainly localizes at the plasma membrane but is also found at the *trans* Golgi⁴⁴. As the enzymatic activity assay in lysates reports on the global sphingomyelin synthesis capacity, we next investigated *de novo* sphingomyelin synthesis that occurs at the *trans* Golgi, where CERT as well as the ORP9-ORP11 dimer localize. For this purpose, we chased the metabolic fate of palmitic acid alkyne (**Fig. 7C**). Palmitic acid is the precursor of sphinganine and all sphingolipids (**Fig. 3B, 7C**). To enter the sphingolipid pathway, palmitic acid first needs to travel to the ER and later to the Golgi for conversion to sphingomyelin, unlike ceramide analogues, such as NBD-ceramide, that can be converted to sphingomyelin by the plasma membrane-resident SMS2. Furthermore, the palmitic acid alkyne does not contain a bulky fluorescent group and the terminal alkyne allows visualization by click chemistry (**Fig. 7C**). As this method enabled us to monitor *de novo* sphingomyelin production in intact cells, we confirmed the reduced *de novo* sphingomyelin synthesis in CERT knockout cells using this method (**Fig. 7D, E, S8C**). In addition, ORP9 and ORP11 knockouts also showed decreased conversion of palmitic acid to sphingomyelin, suggesting a similar defect as CERT knockouts. To confirm the decreased sphingomyelin synthesis, we quantified the Golgi localization of a DAG biosensor, C1ab domain of protein kinase D1, that can report on sphingomyelin synthesis^{45,46}. This showed decreased DAG levels in the Golgi that can be accounted for lowered sphingomyelin synthesis (**Fig. S8D**).

The observations that loss of ORP9 or ORP11 does not affect CERT protein (**Fig. 3E**) or reduce CERT localization to the Golgi (**Fig. S9**) implied that CERT-mediated transfer routes are not affected in ORP9 or ORP11 knockouts. Lipidomics analysis showing accumulation of ceramide and glucosylceramide in ORP9/ORP11 knockouts further suggested the conversion of ER-bound ceramides to sphingomyelin in the Golgi is hampered.

To distinguish between two possibilities that may result in lowered sphingomyelin levels – a ceramide delivery defect to the *trans* Golgi or an inability to convert ceramide to sphingomyelin in the Golgi, we established an immunoisolation protocol for *trans* Golgi membranes using a monoclonal antibody against the *trans* Golgi marker Golgin-97 (**Fig. 7F**). These isolates were enriched for the *trans* Golgi marker Golgin-97 and were devoid of other organelle markers, such as the ER, mitochondria, and lysosomes (**Fig. 7G**). We confirmed the membrane integrity of Golgin-97-enriched fractions by their sphingomyelin synthase activity, as these multi-pass transmembrane proteins require intact membranes for activity⁴⁴ (**Fig. S10A**). Lipidomics analysis of these fractions validated that the loss of ORP11 and especially that of ORP9 results in lowered PS levels in the *trans* Golgi (**Fig. 7H, S10B-D**). The *trans* Golgi fractions also showed reduced sphingomyelin levels, confirming the limited *de novo* sphingomyelin synthesis (**Fig. 7D, E, I, S10E**). Moreover, the same fractions showed elevated ceramide levels in these fractions (**Fig. 7J, S10F**), revealing that the knockouts do not have a ceramide delivery defect, but instead a lowered capacity to convert ceramide to sphingomyelin in their *trans* Golgi membranes. We tested this notion by performing a sphingomyelin synthase activity assay in the isolated Golgi membranes, where supplying excess substrate to these membranes bypasses the ceramide delivery routes (**Fig. 7K, L**). This assay further substantiated that the Golgi of ORP11 and

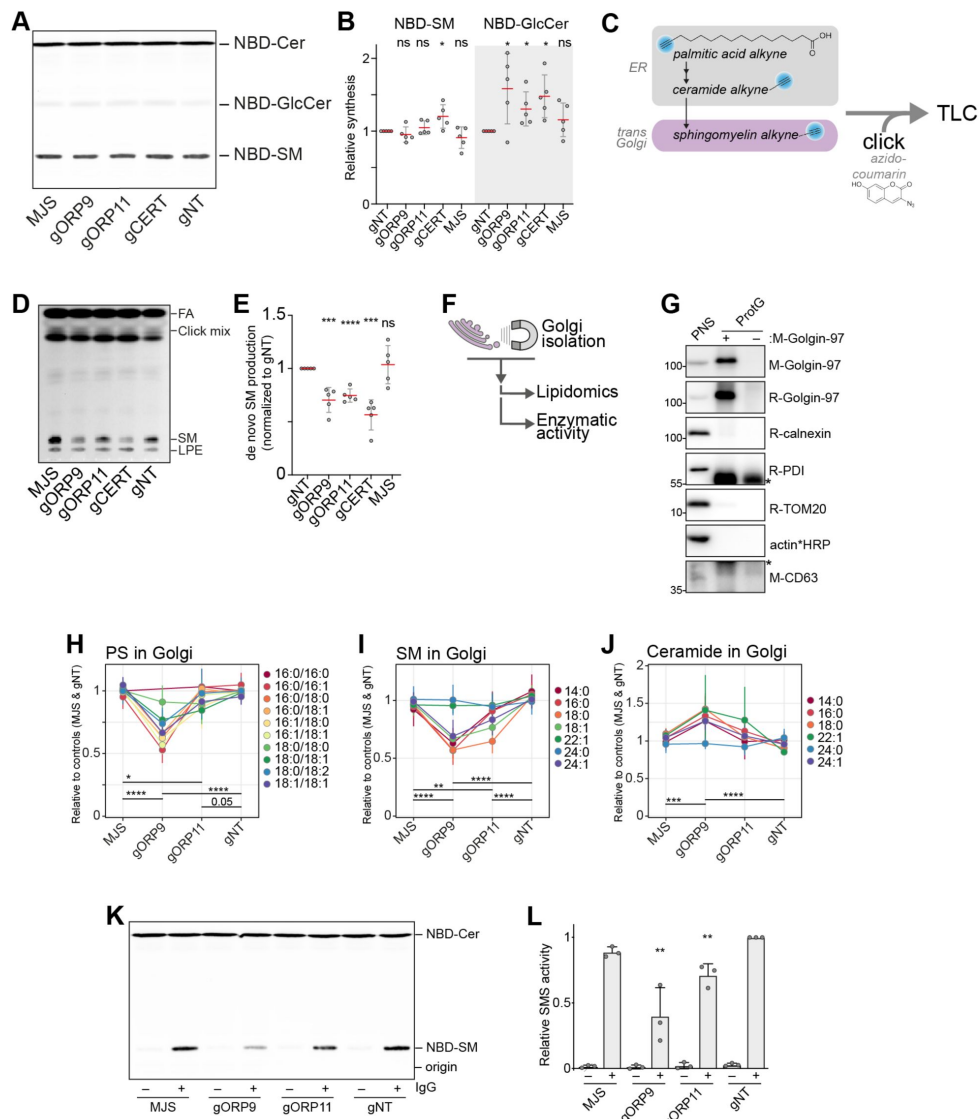


Figure 7

ORP9 and ORP11 are needed for *de novo* sphingomyelin synthesis in the Golgi apparatus.

(A) Thin-layer chromatography readout of the enzymatic activity assay performed in lysates reveals the unreduced sphingomyelin synthesis capacity of knockout cells. (B) Quantification of the enzymatic activity assays corresponding to panel A. Note the increased GlcCer production capacity in the knockout cells. Red lines and error bars correspond to mean and standard deviation from 5 experiments, respectively. (C) Graphic representation of experiments using palmitic acid alkyne for monitoring *de novo* sphingomyelin synthesis. Alkyne modified sphingolipids are “clicked” with azido-coumarin before thin-layer chromatography (TLC) analysis. (D) TLC readout of *de novo* sphingomyelin synthesis assay in intact cells using palmitic acid alkyne. Knockout cells demonstrate reduced conversion of palmitic acid to sphingomyelin. FA: fatty acid, SM: sphingomyelin, LPE: lyso-O-phosphatidylethanolamine (E) Quantification of *de novo* sphingomyelin synthesis assay from panel C. Red lines and error bars correspond to mean and standard deviation from 5 experiments, respectively. (F) Simplified representation of Golgi-targeted lipidomics and enzymatic activity assays. (G) Western blot confirming the immunomagnetic isolation of *trans* Golgi membranes. Cross-reactivity to Protein G and/or Golgin-97 IgG were labeled with asterisks. (H-J) Lipidomics analysis of Golgi isolates show lowered PS levels in the Golgi of ORP9 and ORP11 knockout cells. Same Golgi fractions have reduced sphingomyelin but increased ceramide levels. Each colored line corresponds to a lipid species. Data points and the error bars correspond to mean and standard deviations from 4 experiments. (K) TLC readout of enzymatic activity assay performed in isolated Golgi from knockout cells. Golgi of ORP11 and especially that of ORP9 demonstrate lowered capacity to synthesize sphingomyelin. (L) Quantification of sphingomyelin synthesis activity assay performed in Golgi isolates corresponding to panel I.

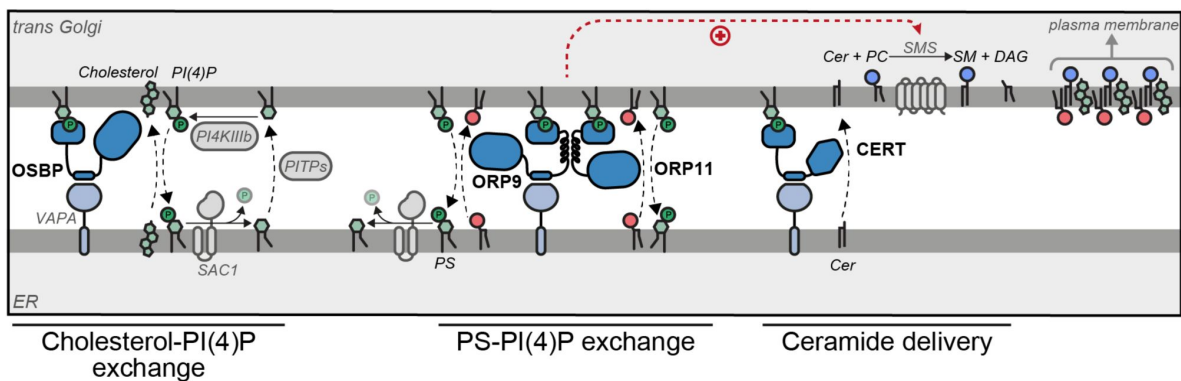


Figure 8

Model of ORP9-ORP11 mediated promotion of sphingomyelin synthesis at the ER-trans Golgi contact site.

ORP9 and ORP11 require dimerization with each other to localize at ER-*trans* Golgi membrane contact sites, where they exchange PS for PI(4)P. Consequently loss of either protein causes PS and PI(4)P imbalances in the Golgi apparatus. Since only ORP9 contains a FFAT motif, its loss leads to a more pronounced effect on PS, PI(4)P and sphingolipid levels. The same contact site accommodates other LTPs. Multiple phosphatidylinositol transfer proteins (PITPs) traffic phosphatidylinositol to the Golgi for their phosphorylation. Each PITP at the ER-Golgi contact site serves a different function—one of these proteins, Nir2, also contains a FFAT motif (ref.46 and 54). OSBP and CERT are responsible for the anterograde trafficking of cholesterol and ceramide, the latter is used for sphingomyelin production. Cholesterol, sphingomyelin and PS are trafficked to the plasma membrane by vesicular means to be asymmetrically distributed between the leaflets of the plasma membrane.

especially of ORP9 knockout cells have a lowered sphingomyelin synthesis capacity. Meanwhile, localization of both sphingomyelin synthases was not reduced in the Golgi, as detected by three different antibodies (Fig. S11). Collectively, our results indicate that PS-PI(4)P exchange between the ER and *trans* Golgi mediated by the ORP9-ORP11 LTP complex is critical for *de novo* sphingomyelin synthesis in *trans* Golgi.

Discussion

In this study, we describe a gene knockout library for systematic characterization of intracellular LTPs. The arrayed design of the library enables high and low throughput analysis. As new LTPs are identified in regular basis, the arrayed feature of the library allows expansion to include newly identified LTPs, e.g. ATG2A, SHIP164, KIAA0100 (Hobbit in *Drosophila*), KIAA1109 (Csf1 in yeast) and RMDN3 are new human LTPs that are identified through the course of this study^{8,10,12,13}.

Lipidomics analysis of the library demonstrated many lipid imbalances. We further validated loss of NPC1, NPC2, CERT, and GLTP with sphingolipid imbalances^{15,18,20} (Fig. 1C). In addition to sphingolipid imbalances, we found STARD7 knockout cells with increased levels of phosphatidylglycerol (PG), a lipid class exclusive to mitochondria in mammals (Fig. 1C). STARD7 is a phosphatidylcholine (PC) transfer protein that localizes to the mitochondrial intermembrane space to supply PC to the mitochondrial inner membrane^{47,49}. Consequently, loss of STARD7 reduces PC levels in this membrane as well as decreasing cardiolipin levels and respiratory capacity^{48,49}. While PC in the inner membrane is not a precursor of cardiolipin, it is possible the reduced PC levels in this membrane impair the activity of the cardiolipin synthase that uses PG as its substrate, suggesting an explanation for the PG accumulation in STARD7 knockout cells.

LTPs often localize at membrane contact sites to facilitate lipid exchanges between organelles. We found ORP9 and ORP11 localizing at the ER-*trans* Golgi contact sites to exchange PS and PI(4)P. We show that the dimerization is critical for the contact site localization, and consequently, loss of either protein is sufficient to disturb PS and PI(4)P levels in the Golgi. In return, this phospholipid imbalance reduces sphingomyelin synthesis capacity of the Golgi. Compared to ORP11 knockout cells, ORP9 knockout cells display more pronounced phenotypes of cellular sphingolipid imbalances (sphingomyelin and glucosylceramide), phospholipid imbalances in the Golgi apparatus (PS and PI(4)P), as well as reduced capacity of sphingomyelin synthesis in *trans* Golgi membranes. Furthermore, loss of ORP9 leads to a more dramatic effect on the Golgi localization of ORP11 than vice versa. This is most likely due to ORP9 providing a critical factor, i.e. the FFAT motif, for contact site localization, whereas it is possible the loss of ORP11 can be partially compensated by ORP10.

The contact site localization of the ORP9-ORP11 dimer is homologous to that of the ORP9-ORP10 dimer localizing at the ER-endosome and ER-Golgi contact sites as ORP10 also uses its coiled coils to interact with ORP9^{35,36}. In both LTP complexes, ORP9 provides the FFAT motif required for ER contact. ORP10 can also deliver PS to Golgi membranes⁵⁰, however, our lipidomics analysis of ORP10 knockout cells did not demonstrate any sphingolipid imbalances (Fig. S12A). Besides ORP9, ORP10 and ORP11, other LTPs are also shown to dimerize at the ER-Golgi interface. A recent structural study has revealed the architecture of a previously-described OSBP dimerization that is mediated by a central core domain containing two alpha helices^{51,52}. CERT forms a similar dimer and the conformational changes dictated by the central core domain is responsible for regulating the activity of the CERT dimer⁵³. Both OSBP and CERT homodimers form a T-shaped structure, dissimilar to the heterodimers of ORP9, ORP10 and ORP11.

What distinguishes ORP11 from ORP10? An analysis of expression profiles from >900 cancer cell types showed that ORP10 and ORP11 are not differentially expressed (Fig. S12B). On the contrary, they show a positive correlation. It is possible that ORP9 interacts with ORP10 or ORP11 in different biological conditions or sub-cellular locations. ER-endosome contact site localization of the ORP9-ORP10 dimer supports this notion³⁵. Even within the Golgi, ORP9-ORP10 and ORP9-ORP11 dimers might be facilitating lipid flows at different sub-organellar domains. The presence of multiple phosphatidylinositol (PI) transfer proteins localized at ER-*trans* Golgi contact sites feeding PI(4)P synthesis in the Golgi for distinct purposes and the observation of different PI(4)P-containing sub-domains in the Golgi promotes the idea that ORPs could localize at different Golgi sub-domains^{55,56}. Furthermore, all three proteins, together with OSBP and ORP1L, are recruited to the lysosomal damage site in response to the increased PI(4)P levels on lysosomal delimiting membrane^{34,57}. Collectively, these reports highlight the spatiotemporally dynamic nature of PI(4)P-mediated lipid trafficking and suggest that the two dimers could have different functions.

An intriguing observation is that the loss of ORP9 causes more accumulation of ceramide than CERT knockouts, despite loss of either protein leading to a comparable reduction of sphingomyelin levels. As the loss of CERT would lead to a ceramide accumulation in the ER, it is possible that such an accumulation in the ER is sensed to reduce ceramide production in this organelle. An ER-resident candidate ceramide sensor for this purpose was suggested previously⁵⁸. Meanwhile, our findings show a ceramide accumulation in the *trans* Golgi of ORP9 knockouts. Accordingly, ceramide accumulation in the Golgi caused by the loss of ORP9 would fail to “turn on” an ER-localized ceramide sensing machinery, thus leading to further ceramide accumulation compared to CERT knockout cells. This notion also supports our finding that the loss of the ORP9-ORP11 dimer causes ceramide accumulation primarily in the Golgi.

Asymmetric distribution of lipids between two bilayer leaflets is a characteristic feature of the plasma membrane. This is owed to the build-up of sphingomyelin and cholesterol on the outer leaflet and PS on the inner leaflet¹⁴. The transition of the thin, symmetrical ER membrane to a thicker, rigid and asymmetrical one takes place in the Golgi (Fig. 8)¹⁴. Sphingolipid, cholesterol and PS concentrations also increase along the secretory pathway. Various mechanisms are described to drive the sphingolipid and cholesterol trafficking against the concentration gradient, including thermodynamic trapping of cholesterol due to complex formation with sphingomyelin or energy release from the retrograde trafficking of PI(4)P followed by its hydrolysis in the ER^{14,31,59}. The same PI(4)P gradient between the ER and Golgi could also power the anterograde trafficking of PS, which, unlike sphingomyelin or cholesterol, is still exposed on the cytosolic leaflet of the Golgi where it has a higher concentration than the ER – thus, maintaining lipid trafficking against the gradient requires energy. In brief, our finding that the ORP9-ORP11-dimer-mediated phospholipid exchange promoting the sphingomyelin synthesis reveal further intertwining of lipid gradients along the secretory pathway at the ER-*trans* Golgi membrane contact sites.

Conflict of Interest

Authors declare no conflict of interest.

Acknowledgements

Authors thank Ruud Wijdeven, Robbert Q. Kim of LUMC protein facility, Carolina Jost and the members of the Neeffjes lab for their technical and critical input. Authors are especially grateful to Joost Holthuis and Matthijs Kol of University of Osnabrück for their intellectual input.

Materials and methods

Cell culture

MelJuSo and HEK293T (ATCC CRL-3216) cells were cultured in IMDM (Gibco #21980) and DMEM (Gibco #41966) supplemented with 8% fetal calf serum (Biowest #S1810), respectively. MelJuSo cell line authentication was performed by Eurofins Genomics (19-ZE-000487).

Library design, generation and transduction

Targeting and non-targeting guide sequences (Supplementary Table 1) were obtained from the Brunello Human CRISPR Knockout Pooled Library⁶⁰ and cloned into lentiCRISPR v2 plasmid⁶¹ as described previously⁶². Cloning of guide RNAs were individually confirmed by Sanger sequencing.

For library transduction, HEK cells were seeded on a 96-well plate on the day before transfection and transfected with library plasmids and lentiviral packaging plasmids pRSVrev, pHCMV-G VSV-G, and pMDLg/pRRE using polyethyleneimine (Polysciences #23966). A day after replacing the medium, virus was harvested and MelJuSo cells were transduced in the presence of 4µg/ml polybrene (EMD Milipore #TR-1003-G). Transduced cells were subjected to selection using 2µg/ml puromycin.

Lipid extractions and lipidomics analysis

For lipidomics analysis, library-generated cells were expanded to 15-cm dishes and cultured in IMDM supplemented with lipid-depleted serum (Pel-Freez #37217-5) for 3-4 days. Next, cells were scraped in 2% NaCl solution and lipids were extracted following the Bligh-Dyer protocol. In brief, harvested cells were resuspended in 200µL 2% (w/v) NaCl followed by addition of 500µL methanol and 250µL chloroform. Samples were vortexed for 5 min. Following phase separation by adding 250µL chloroform and 250µL 0.45% (w/v) NaCl, samples were centrifuged for 5min at 15,000xg. Next, bottom fractions were collected and dried under continuous nitrogen stream.

Comprehensive, quantitative shotgun lipidomics was carried out as described in detail elsewhere^{63,64}. Briefly, dried lipid extracts were spiked with 54 deuterated internal standards and dissolved in methanol:chloroform 1:1 containing 10 mM ammonium acetate. Lipids are then analysed with a flow injection method at a flow rate of 8 µL/min applying differential ion mobility for lipid class separation and subsequent multiple reaction monitoring in positive and negative electrospray ionization mode. Using the Shotgun Lipidomics Assistant (SLA) software individual lipid concentrations are calculated after correction for their respective internal standards.

Data analysis and statistics

Data analyses, including lipidomics data analysis, were performed using R (4.1.0 “Camp Pontanezen”) and RStudio (2022.12.0+353) with following packages: *ggplot2*, *dplyr*, *readr*, *ggrepel*, *ggcorrplot2*, *reshape2*, *ggsignif*, *purrr*, *tidyr*, and *tibble*. For Z-score calculations, first the percentages of each lipid class within individual measurements were calculated, followed by calculating Z-scores for individual data points using the following formula: “ $Z = (x - \mu)/\sigma$ ”, where μ is the mean percentage of a lipid class and σ is the standard deviation. Next, average Z-scores for LTP knockout cell lines were calculated. For POPC normalized data analysis for the analysis of acyl chain distributions and Golgi lipidomics, each lipid subspecies normalized to palmitoyl-oleoyl-phosphatidylcholine (POPC) levels. For Golgi lipidomics, POPC-normalized values were normalized again to the mean of POPC-normalized values for MJS and gNT samples. Raw lipidomics data available at Supplementary Table 2.

Mean values are denoted in all graphs except for boxplots. When present, error bars indicate standard deviations. In boxplots, middle line denotes median, box boundaries denote the first (Q1) and third (Q3) quartiles, and the lower and upper whiskers denote “ $Q1-1.5*IQR$ ” and “ $Q3+1.5*IQR$ ”, respectively. IQR: inter-quartile range. For statistical analysis, student’s t-test is used, unless stated otherwise. * $p<0.05$, ** $p<0.01$, *** $p<0.001$, **** $p<0.0001$.

Co-immunoprecipitation, SDS-PAGE and Western blotting

Co-immunoprecipitation from HEK293T cells, SDS-PAGE and Western blotting were performed as described previously²⁷[↗](#).

Immunofluorescence staining and quantifications

For equinatoxin staining, cells were fixed with 4%PFA:PBS (v/v) and permeabilized with 10 μ g/ml digitonin in PBS for 15min at RT. Further stainings were performed in PBS. PI4P staining was performed after fixation in 2% PFA/PBS for 15 minutes followed by permeabilization with 20 μ M digitonin in Buffer A (20mM PIPES, pH 6.8, 137mM NaCl and 2.7mM KCl). Blocking was performed in Buffer A supplemented with 5% (v/v) serum. Next, cells were incubated with the PI(4)P antibody and the anti-mouse IgM secondary antibody, respectively—both diluted in blocking solution. Cells were washed with buffer A and fixed in 2% PFA/PBS for 5 minutes. Coverslips were mounted on slides using Vectashield Vibrance (Vector Laboratories #H- 1700). All other immunofluorescence staining was performed as described previously²⁷[↗](#).

Images were acquired using a Zeiss LSM 900 with Airyscan. Images were analysed and quantified using ImageJ/FIJI software. To quantify the Golgi localization of lipid biosensors (OSBP-PH, LactC2 and C1ab), first a mask was created using Golgin-97 counter staining and this mask was used to quantify signal from *trans* Golgi as well as the cytoplasm. Golgi localization of immunofluorescence staining of endogenous proteins (ORP9, ORP11, CERT) and the PI(4)P antibody was performed first by creating a mask using Golgin-97 and later using this mask to quantify signal of interest relative to signal of Golgin-97. Manders’ coefficient for colocalization was calculated using the Jacop plugin for ImageJ/FIJI.

Flow cytometry analysis

MeJJuSo cells were brought to suspension by trypsinization and stained with the indicated probes on ice prior to analysis using a BD LSR-II equipped with 488 and 561nm lasers. Data was analysed using FlowJo v.10 software.

Electron microscopy

Cells cultured in 6-cm dishes were fixed for an hour at room temperature by adding double concentrated fixative to the medium (final concentration: 1.5% glutaraldehyde in 0.1M cacodylate buffer). After three times rinsing with 0.1 M cacodylate buffer, the cells were postfixated with 1% osmium tetroxide and 1.5% uranyl acetate. Cells are dehydrated with a series of ethanol, followed by a series of mixtures of ethanol and EPON (LX112, Leadd) and at the end pure EPON. BEEM capsules filled with EPON were placed on the dishes with the open face down. After EPON polymerization at 40°C the first night and 70°C the second night, the BEEM capsules were snapped off. Ultrathin sections 80 nm were made parallel to the surface of the BEEM capsules containing the cultured cells. The sections were contrasted with uranyl acetate and lead hydroxide and examined with a Tecnai Twin transmission electron microscope (Thermo Fisher, Eindhoven, Netherlands). Overlapping images were automatically collected and stitched together into a composite image as previously described⁶⁵[↗](#).

Recombinant protein expression and purification

A codon optimized version of cDNA encoding the non-toxic version of equinatoxin²² was ordered from IDT technologies, GFP sequence was obtained from meGFP-C1 vector and a cDNA encoding the fusion protein was synthesized using Gibson Assembly. A codon optimized version of cDNA encoding the PH domain of FAPP1 containing the T13C, C37S, and C94S mutations were ordered from IDT technologies. cDNA encoding human VAPB gene was described previously²⁷. cDNAs encoding ORD domains of ORP9 and ORP11, VAPB without its C-terminal transmembrane helix, FAPP1-PH, and EQT-GFP fusion protein were cloned into a pNKI1.8/GST-expression vector.

For FAPP1-PH and VAPB-His expressions *E. coli* BL21 was grown in LB medium and expression was induced when OD₆₀₀ was at 0.6 for overnight at 18°C. For other proteins, *E. coli* BL21/Rosetta were grown in 2xYT medium and expression was induced when OD₆₀₀ was at 1 for overnight at 18°C. Bacterial pellets were resuspended in GST purification buffer (50mM Tris pH 8.0, 250mM NaCl, 1mM EDTA, 1mM DTT) and lysed by tip sonication. Lysates were cleared by centrifugation at 12,000xg for 30 min. Proteins were purified using Glutathione Sepharose™ 4 Fast Flow (GE Healthcare #17-5132-03) and cleaved using 3C protease protein prior to reverse purification using glutathione beads followed by a HiLoad 16/60 Superdex 75 size exclusion chromatography.

Full-length ORP9 and ORP11 were expressed using a baculovirus expression in *Spodoptera frugiperda* (Sf9) using an adapted Bac-to-Bac system (Invitrogen). In brief, cDNAs were cloned to an in-house insect expression vector and bacmids were generated using EmBacY cells (Geneva Biotech) isolated using isopropanol precipitation. 10 µg Bcmid was transfected to sedentary Sf9 cells using CellFectin (Invitrogen) in SFM-II medium (Gibco) in a 6-well plate at 28 °C. Virus-containing medium was harvested (P0) after 72 hours for infection of 10⁶ cells in Insect-Express medium (Lonza) to be cultured at 28°C while constant shaking. Cells were harvested by centrifugation after 72 hours and purified using Strep-Tactin Sepharose beads (iba #2-1201-010).

NBD-labelling of FAPP1-PH

Labelling of FAPP1-PH was performed according to ref.³⁷. In brief, purified protein was incubated with 5-fold excess IANBD-amide overnight (Setareh Biotech #6281) followed by quenching of unbound dye with L-cysteine 5-fold excess of the dye. Next, labelled protein was subjected to Zeba Spin desalting column (Thermo Fisher #89890). Labelling efficiency was determined by absorbances at 280nm and 480nm using a NanoDrop.

Methyl-β-cyclodextrin and MTT viability assay

Cells were seeded in a 96-well plate and were cultured in OptiMEM (ThermoFisher #31985047) for 3 days. Cells were treated with 10mM methyl-β-cyclodextrin (Sigma #C4555) and cell viability was tested using MTT viability assay (Cayman #21795). Absorbance at 560nm was measured using a BMG ClarioStar plate reader.

Liposome preparations

For PS transfer assay using ORDs, donor liposomes composed of 2% NBD-PS (Avanti #810194), 2% Rhodamine-PE (Avanti #810150), 10% DOPE (Avanti #850725), 86% DOPC (Avanti #850375) and acceptor liposomes composed of DOPC with or without 5% brain PI(4)P (Avanti #840045) were used. For PS transfer assays using full-length proteins, donor liposomes composed of 2% NBD-PS, 2% Rhodamine-PE, 2% 18:1 DGS-NTA(Ni) (Avanti# 790404), 10% POPE (Avanti # 850757) and 84% POPC (Avanti #850457) and acceptor liposomes of 85% POPC, 10% POPE and 5% brain PI4P were used. For PI4P transfer assays, donor liposomes were 95% DOPC and 5% POPS (Avanti # 840034) and acceptor liposomes were 93% DOPC and 5% PI4P (Echelon #P-4016), and 2% Rhodamine-PE.

Lipids were mixed in a glass container and dried under a constant nitrogen flow to create a film. Lipids were freeze-dried at least for two hours under vacuum. Next, lipid films were rehydrated in HKM (50mM HEPES pH 7.2; 120mM potassium acetate; 1mM MgCl₂) buffer for 30 minutes followed by 5 cycles of freeze thaw. Lipids were extruded using Avanti MiniExtruder using a 100nm or 200nm filter. Uniformity of lipids were confirmed using a Wyatt Nanostar Dynamic Light Scattering.

Lipid transfer assays

For PS transfer assays using ORDs, final concentrations of 80μM of each donor and acceptor vesicles were used in 100μL volume and the indicated amounts of protein of interest was added in 5μL. NBD fluorescence in time was measured using a BMG ClarioStar plate reader. For PS transfer assay using full-length proteins, 100μM of each donor and acceptor vesicles were used with 150nM ORP9, 150nM ORP11 and 450nM VAPB-His. Maximum rate of transfer (V_{max}) was calculated using a self-starting non-linear least squares function implemented in R (SSmicmen) after background subtraction to no protein control and normalizing to maximum amount of fluorescence obtained after addition of 2% CHAPS. PI4P transfer assay were adapted from ref.³⁷. Donor and acceptor liposomes were first incubated with 500nM NBD-labelled FAPP1-PH for 5 minutes before addition of 150nM ORD9 or ORD11. Data was fit using a self-starting non-linear least squares function implemented in R (SSmicmen).

Liposome floatation

10μM VAPB-His was incubated 360μM liposomes containing NTA-DGS lipids in 100μL HKM buffer for 30min at RT before mixing with 0.3mL HKM buffer containing 54% sucrose to obtain final concentration of 40.5% sucrose. Samples were laid at the bottom of an ultracentrifuge tube and cushioned with HKM buffer containing 30% and 0% sucrose. Samples were centrifuged at 200,000xg for 2 hours at 4°C and fractions were collected for Coomassie blue staining.

Liposome tethering

100nM of each ORP9, ORP11 and VAPB-His were incubated with donor and acceptor liposomes for 1h at RT. Diameter of liposomes were measured using a Wyatt Nanostar Dynamic Light Scattering.

AlphaFold & AlphaFold-multimer predictions

Structure predictions were performed using AlphaFold, AlphaFold-Multimer and ColabFold prediction tools, as described⁶⁶–⁶⁸.

Golgi isolation and quantification of Golgi lipid levels

Cells were washed twice with 0.25M Sucrose and scraped in IM buffer (0.25M Mannitol, 0.5mM EGTA, 5mM HEPES pH 7.4). Samples were passed through a 26xG needle for lysis. Lysates were cleared from nuclei by centrifugation twice at 600xg for 5min. Post-nuclear supernatant was subjected to protein determination using BCA protein determination kit. Equal amounts of protein were supplemented with 150mM NaCl and incubated with Protein A/G Magnetic Beads (ThermoFisher #88802) preloaded either or not with Golgin-97 antibody. Next, samples were washed 3 times with IM buffer supplemented with 150mM NaCl before lipid extraction for lipidomics analysis (described above) or enzymatic activity assay (described below). Amounts of Golgi fractions isolated from different knockouts were confirmed by western blotting.

siRNA transfections and metabolic chasing of BODIPY-C5-ceramide in intact cells

siRNA transfections were carried out as described previously²⁷. siRNA for UGCG (M-006441-02-0005) and UGT8 (M-010270-02-0005) were obtained from Horizon Discovery. MeJuso cells treated with siRNAs or 10 μ M PDMP (Cayman #62595) were washed twice with PBS and incubated with serum-free medium supplemented with 0.25 μ M BODIPY-C5-Ceramide complexed to BSA (Thermo Fisher #B22650). After 3 hours, cells were subjected to lipid extraction and thin layer chromatography as described below. The following lipids were used as standards: TopFlour-C11-galactosylceramide (Avanti Polar Lipids #810266), TopFlour-C11-glucosylceramide (Avanti Polar Lipid #810267) and BODIPY-C5-Lactosylceramide (Thermo Fisher #B34402).

Metabolic chasing of de novo sphingomyelin synthesis

Cells were incubated with 20 μ M ethanolic palmitic acid alkyne (Cayman Chemical #13266) in serum-free medium for 6 hours. Next, cells were washed twice in PBS and scraped in 2%NaCl solution. Lysates were subjected to protein determination using Pierce BCA Protein Kit (Thermo #23225) and equal amounts of proteins were used for lipid extractions as above. For alkaline hydrolysis, dried lipids were resuspended in 200 μ L methanolic sodium methoxide and incubated at room temperature for 1h. Samples were added 30 μ L acetic acid/water (1:4, v/v), 120 μ L 2% NaCl, and 400 μ L chloroform to re-extract lipids. Dried lipids were resuspended in 15 μ L chloroform and 65 μ L of click mix containing 400 μ M 3-Azido-7-hydroxycoumarin (Baseclick #BCFA-047-1) and 900 μ M tetrakis(acetonitrile)copper(I) tetrafluoroborate (Sigma #677892) in acetonitrile/ethanol (7:3, v/v) was added and incubated 3h at 45°C prior to TLC analysis.

Quantitative RT-PCR

RT-PCR was performed as described previously²⁷ using the following primer sets:

CERT_1: ATGTCGGATAATCAGAGCTGGA / ATCCTGCCACCCATGAATGTA,

CERT_2: TCCATCTGTCTTAGCAAGGCT / GCTGTTCAATGGCATCTATCCA,

SMS1_1: TGTGCCGAGTCTCCTCTGA / CCGTCTTGTGTGCTTCCAAA,

SMS1_2: CAGCATCAAGATTAACCCAACG / TGGTGAGAACGAAACAGGAAAG,

SMS2_1: TCCTACGAACACTTATGCAAGAC / CCGGGTACTTTTTGGTGCCCT,

SMS2_2: CAAATTGCTATGCCCACTGAATC / GTTGTC AAGACGAGGTTGAAAAC

Enzymatic activity assay in lysates and isolated Golgi fractions

For enzymatic activity measurements in lysates, cells were washed twice in 0.25M Sucrose and scraped in IM buffer (0.25M Mannitol, 0.5mM EGTA, 5mM HEPES pH 7.4). Samples were passed through a 26xG needle for lysis. Lysates were cleared from nuclei by centrifugation twice at 600xg for 5min. Post-nuclear supernatant was subjected to protein determination using BCA protein determination kit. Equal amounts of protein in a 50 μ L volume were mixed with 50 μ L IM buffer supplemented with 5 μ M NBD-C6-ceramide (Avanti Polar Lipids #8102109) from an ethanolic solution. Reactions were incubated 1h at 37°C in dark with constant shaking. Next, samples were subjected to lipid extractions and thin-layer chromatography as described. For the enzymatic activity assays in Golgi, isolated Golgi fractions were resuspended in 50 μ L IM buffer and incubated with NBD-C6-ceramide as above.

Thin-layer chromatography

Dried lipids were spotted on a thin-layer chromatography (TLC) Silica gel 60 (Merck #1.05554.0001) plate and developed in chloroform:methanol:acetone:acetic acid:water (50:10:20:10:5, v/v/v/v/v). Fluorescent images were acquired using a Typhoon FLA9500 equipped with a 488nm laser and a BPB1 filter (530DF20).

Gene expression analysis

Gene expression profiles from 947 cancer cell lines were obtained from the Cancer Cell Line Encyclopedia⁶⁹.

Plasmids

Plasmid	Reference	cDNA	Backbone
GST-EQT-GFP	This study	IDT GeneBlock	pNK11.8
Scarlet-ORP9 iso.2	This study	Mouse Osbp19 isoform 2 cDNA was ordered from Horizon Discovery. BC023759. IMAGE:5344071	mScarlet-C1
Scarlet-ORP11		Human OSBPL11 cDNA was ordered from Horizon Discovery. IMAGE:3916115. BC065213	mScarlet-C1

GFP-OSBP-PH	addgene #49571, ref. ⁴²		
RFP-LactC2	addgene#74061, ref. ⁴¹		
mCherry-PKD/C1ab	addgene# 139314, ref. ⁷⁰		
GFP-CC11	This study		
Mito-tagRFP	This study	cDNA encoding the first 70 amino acids of TOM70 was ordered from IDT technologies.	tagRFP-N1
Mito-CC9-tagRFP	This study		tagRFP-N1
GFP-PH9	This study		meGFP-C1
GFP-PH11	This study		meGFP-C1
GFP-PH9-PH11	This study		meGFP-C1
FLAG-ORP11	This study		FLAG-C1
GST-ORD9	This study		pNK11.8
GST-ORD11	This study		pNK11.8
GST-FAPP1-PH	This study	IDT GeneBlock	pNK11.8
GST-VAPB Δ TM-His	This study	Ref. ²⁷	pNK11.8
Strep-ORP9	This study		
Strep-ORP11	This study		
FLAG-VAPA	Ref. ²⁷		
meGFP-C1	Ref. ²⁷		
mScarlet-C1	Ref. ²⁷		
GFP-VAPA	Ref. ²⁷		
GFP-VAPA**	Ref. ²⁷		
Scarlet-CERT	Ref. ²⁷		

Antibodies

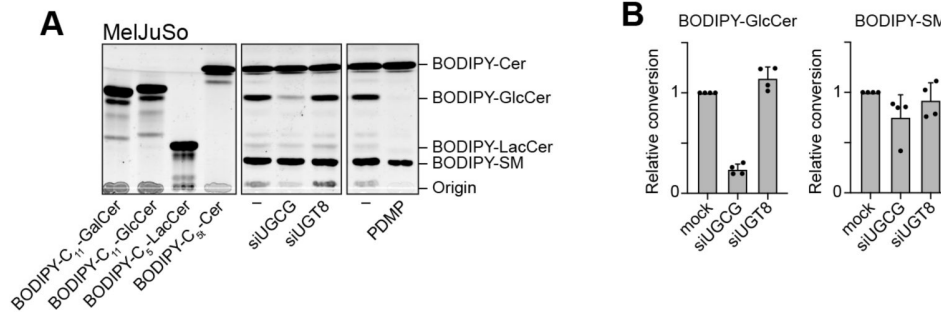
Target	Supplier	Catalog #	Host
OSBP	Proteintech	11096-1-AP	Rabbit
ORP1L	PMID: 12631712		Rabbit
CERT	Bethyl	A300-669A	Rabbit
NPC1	Novus	NB400-148	Rabbit
NPC2	Proteintech	19888-1-AP	Rabbit
GLTP	Proteintech	10850-1-AP	Rabbit
PITPNB	Proteintech	13110-1-AP	Rabbit
ORP9	Proteintech	11879-1-AP	Rabbit
STARD7	Proteintech	15689-1-AP	Rabbit
SEC14L1	Proteintech	25541-1-AP	Rabbit
PITNM1	Proteintech	26983-1-AP	Rabbit
SEC14L2	Origene	TA503723	Mouse
TEX2	Bethyl	A304-705A	Rabbit
FAPP2	Proteintech	15410-1-AP	Rabbit
ORP9	Santa Cruz	sc-398961	Mouse
CD63-V450	BD Horizon	561984	Mouse
CTB-Alexa568	Invitrogen	C34777	
Actin	Sigma-Aldrich	A5441	Mouse
GM130	BD Transduction	610823	Mouse
FLAG-HRP	Sigma-Aldrich	A8592	Mouse

GFP	Ref. ²⁷		Rabbit
Scarlet	ChromoTek	6G6-100	Mouse
tagRFP	Evrogen	AB232	Rabbit
Golgin-97	Invitrogen	A-21270	Mouse
Golgin-97	Cell Signaling	13192S	Rabbit
Calnexin (C5C9)	Cell Signaling	2679	Rabbit
R-PDI	Cell Signaling	3501	Rabbit
TOM20	Proteintech	11802-1-AP	Rabbit
Actin*HRP	Santa Cruz	sc-47778	Mouse
SMS1	Sigma/Aldrich	HPA045191	Rabbit
SMS2	Santa Cruz	sc-293384	Mouse
CERT	Proteintech	15191-1-AP	Rabbit
SMS1	Proteintech	19050-1-AP	Rabbit
ORP11	Proteintech	11318-1-AP	Rabbit
Anti-mouse Alexa 488	Thermo Fisher	A21202	Donkey
Anti-mouse Alexa 568	Thermo Fisher	A10037	Donkey
Anti-mouse Alexa 647	Thermo Fisher	A21236	Goat
Anti-rabbit Alexa 488	Thermo Fisher	A21206	Donkey
Anti-rabbit Alexa 568	Thermo Fisher	A10042	Donkey
Anti-rabbit Alexa 647	Thermo Fisher	A31573	Donkey
Anti-Mouse IgG, HRP	Thermo Fisher	G21040	Goat
Anti-Rabbit, IgG, HRP	Thermo Fisher	G21234	Goat
Anti-Mouse IgM, Alexa Fluor 488	Thermo Fisher	A-21042	Goat
Anti-PtdIns(4)P	Echelon	Z-P004	Mouse IgM

Supplementary Figure 1

Glucosylceramide is the main hexosylceramide in MelJuSo cells.

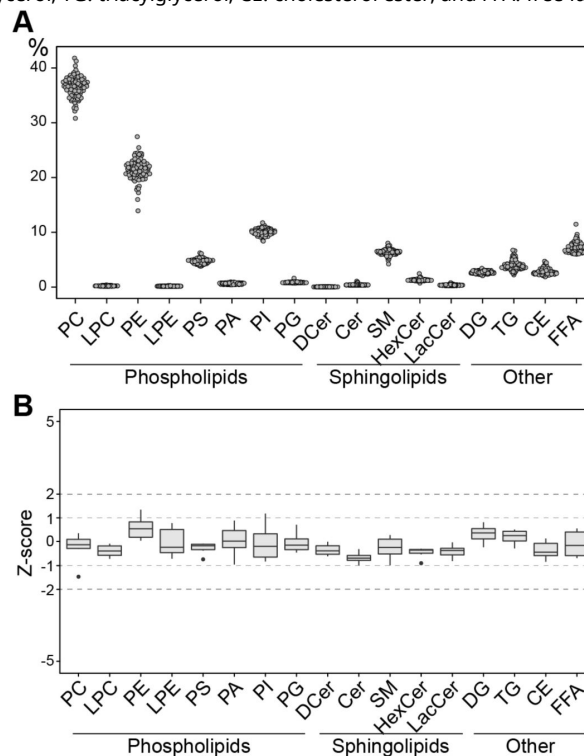
(A) MelJuSo cells silenced for glucosylceramide synthase (siUGCG) or galactosylceramide synthase (siUGT8) or treated with the glucosylceramide synthase inhibitor (PDMP) were fed with the fluorescent ceramide analog BODIPY-C5-ceramide. Lipids were isolated and separated by thin-layer chromatography. Note that the fluorescent band corresponding to monohexosylceramide is affected only when glucosylceramide synthesis is perturbed. (B) Quantifications corresponding to panel A. Bars and error bars correspond to mean and standard deviations from 4 experiments, respectively.

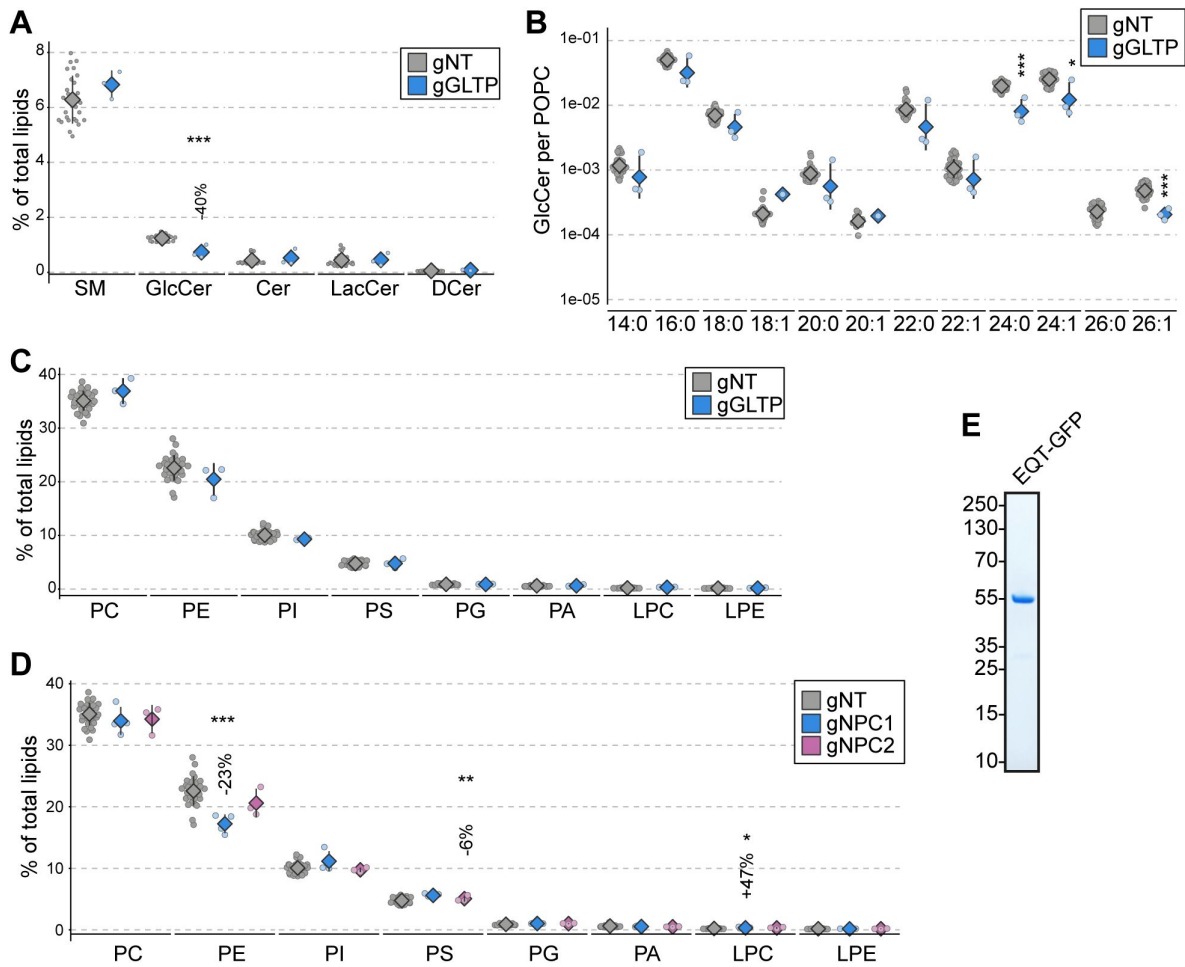


Supplementary Figure 2

Overview of lipidomics analysis performed for LTP knockout library.

(A) Percentage distribution of 17 lipid classes in LTP knockout cells; each data point represents the mean percentage of an LTP knockout cell line. (B) Box plots of Z-scores of NT control cells. Note that Z-scores for NT control cells do not exceed the absolute value of 2. PC: phosphatidylcholine, LPC: lysophosphatidylcholine, PE: phosphatidylethanolamine, LPE: lysophosphatidylethanolamine, PS: phosphatidylserine, PA: phosphatidic acid, PG: phosphatidylglycerol, PI: phosphatidylinositol, DCer: dihydroceramide, Cer: ceramide, SM: sphingomyelin, HexCer: hexosyl-ceramide, LacCer: lactosylceramide, DG: diacylglycerol, TG: triacylglycerol, CE: cholesterol ester, and FFA: free fatty acid.

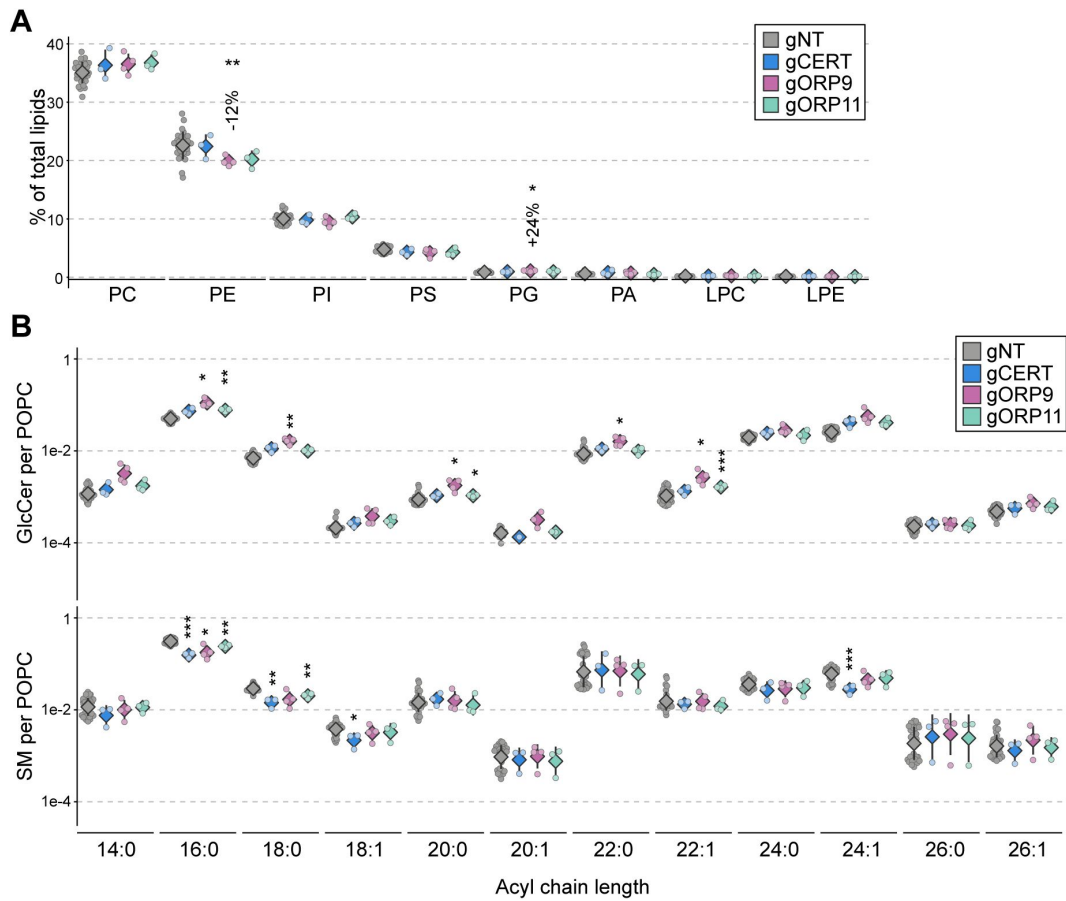




Supplementary Figure 3

GLTP, NPC1 and NPC2 knockout cells do not display major phospholipid imbalances.

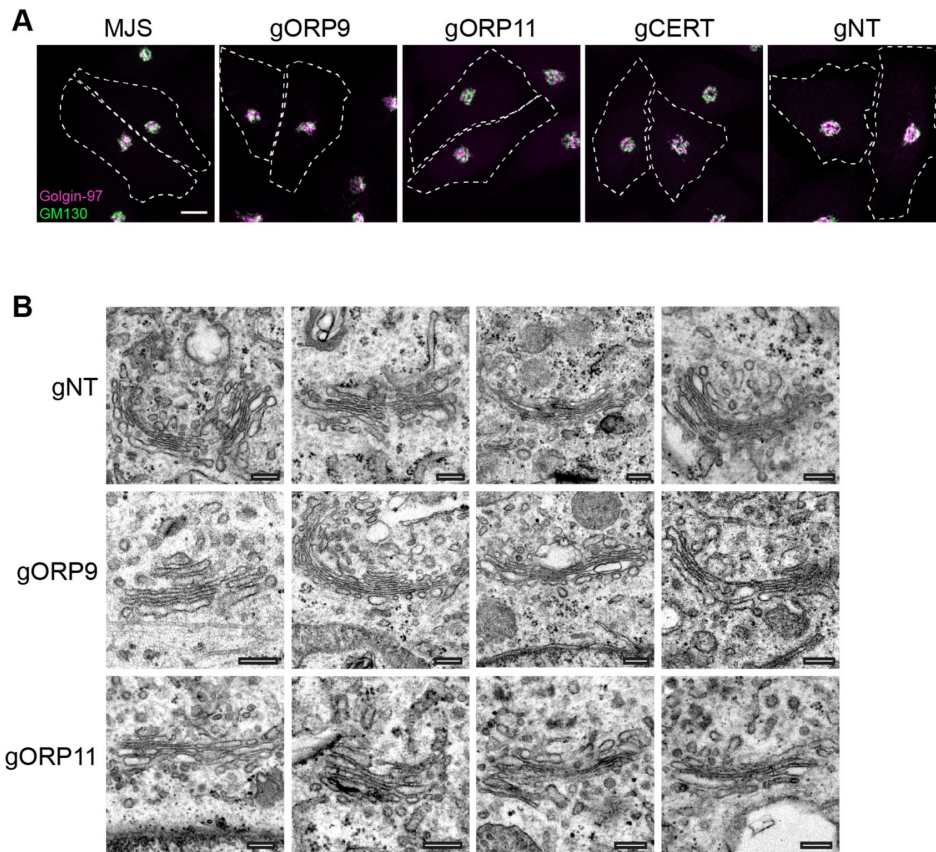
(A, B) Lipidomics analysis of GLTP knockouts show lowered glucosylceramide levels that is represented in various acyl chain species. (C) GLTP knockouts do not present altered phospholipid levels. (D) Lipidomics analysis of NPC1 and NPC2 knockout cells do not display major changes in their phospholipid repertoire. (E) Coomassie Blue staining of recombinant EQT-GFP.



Supplementary Figure 4

Spingolipid imbalances in CERT, ORP9 and ORP11 knockouts are represented in multiple acyl chain species.

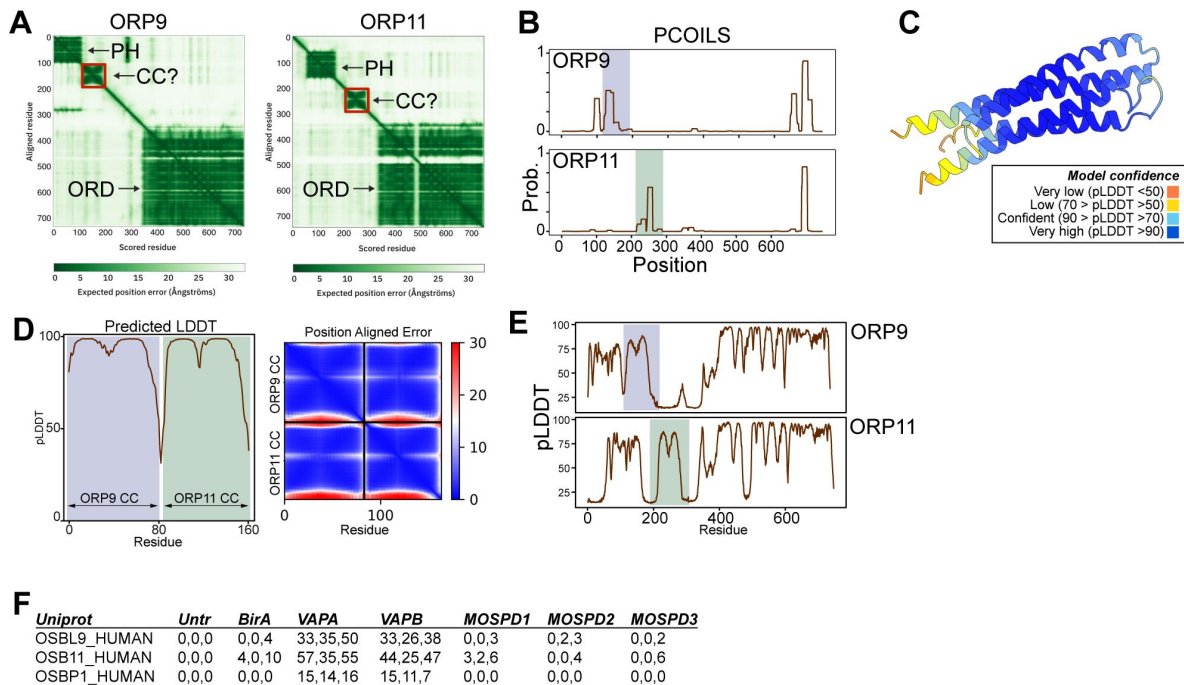
(A) CERT, ORP9 and ORP11 knockouts do not display major phospholipid imbalances. (B) Reduced sphingomyelin and increased glucosylceramide levels in CERT, ORP9 and ORP11 knockout cells is observed in multiple acyl chain species. Lipid levels are normalized to the POPC (16:0/18:1) levels.



Supplementary Figure 5

CERT, ORP9 and ORP11 knockouts do not display defects in Golgi morphology.

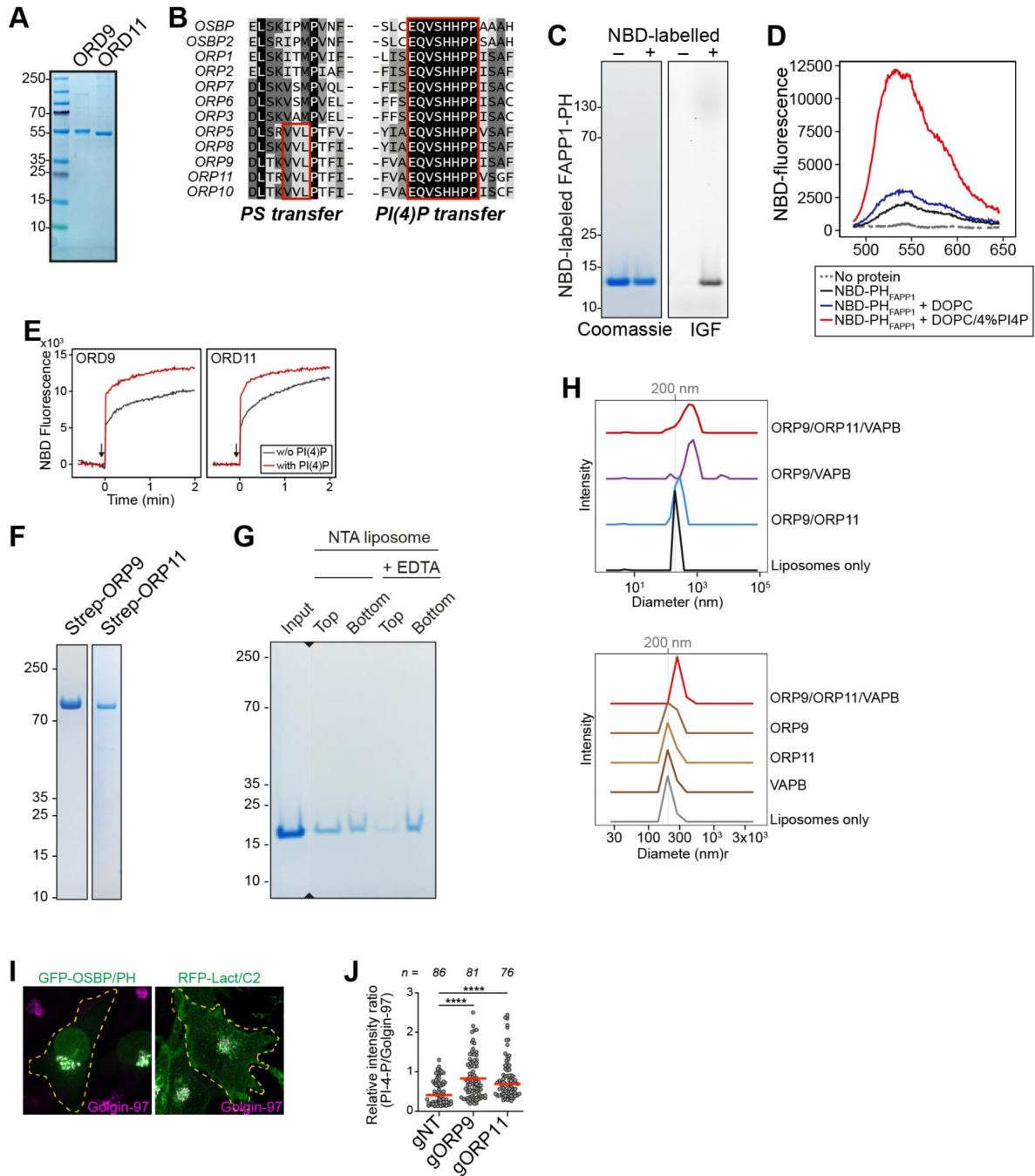
(A) Immunofluorescence staining for *cis* and *trans* Golgi markers, GM130 and Golgin-97 respectively, do not show any changes in ORP9, ORP11 and CERT knockouts. Scale bar 10 μ m. (B) Electron microscopy images for ORP9 and ORP11 knockouts do not display any changes in Golgi morphology. Scale bar 250nm.



Supplementary Figure 6

ORP9 and ORP11 interact with each other via their coiled coils.

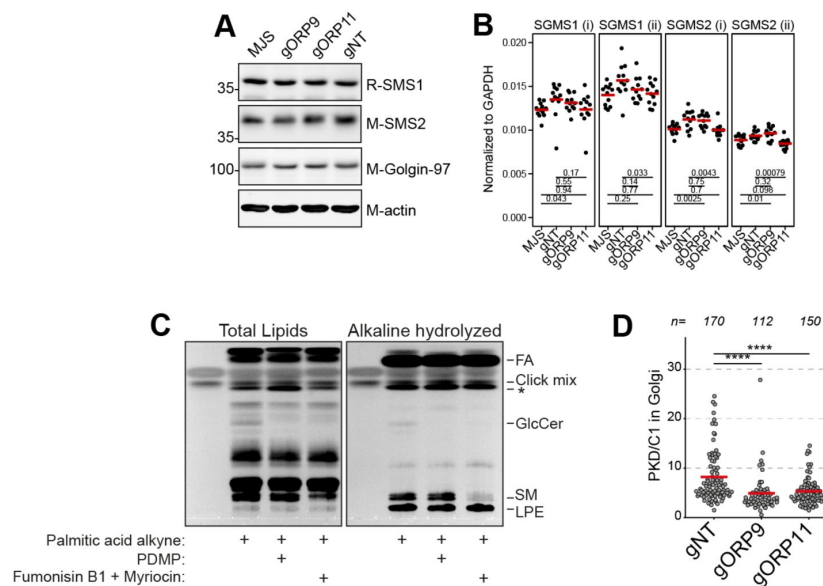
(A) AlphaFold prediction of ORP9 and ORP11 reveals secondary structures between their PH and ORD domains. (B) PCOILS predicts coiled coils in the same of both proteins. Residues corresponding to coiled coils are highlighted. (C) AlphaFold-multimer / ColabFold prediction for ORP9-ORP11 coils dimerization. (D) Predicted local distance difference test (pLDDT) and position aligned error plots for panel C. (E) Predicted local distance difference test for [figure 4C](#). (F) Unique peptide counts from BioID experiments performed with VAPA, VAPB, MOSPD1, MOSPD2, and MOSPD3 from Cabukusta *et al.* 2020. Both ORP9 and ORP11, despite latter lacking a FFAT motif, detected in BioID experiments with VAPA and VAPB.



Supplementary Figure 7

ORP9 and ORP11 are needed for maintaining phospholipid levels in the Golgi.

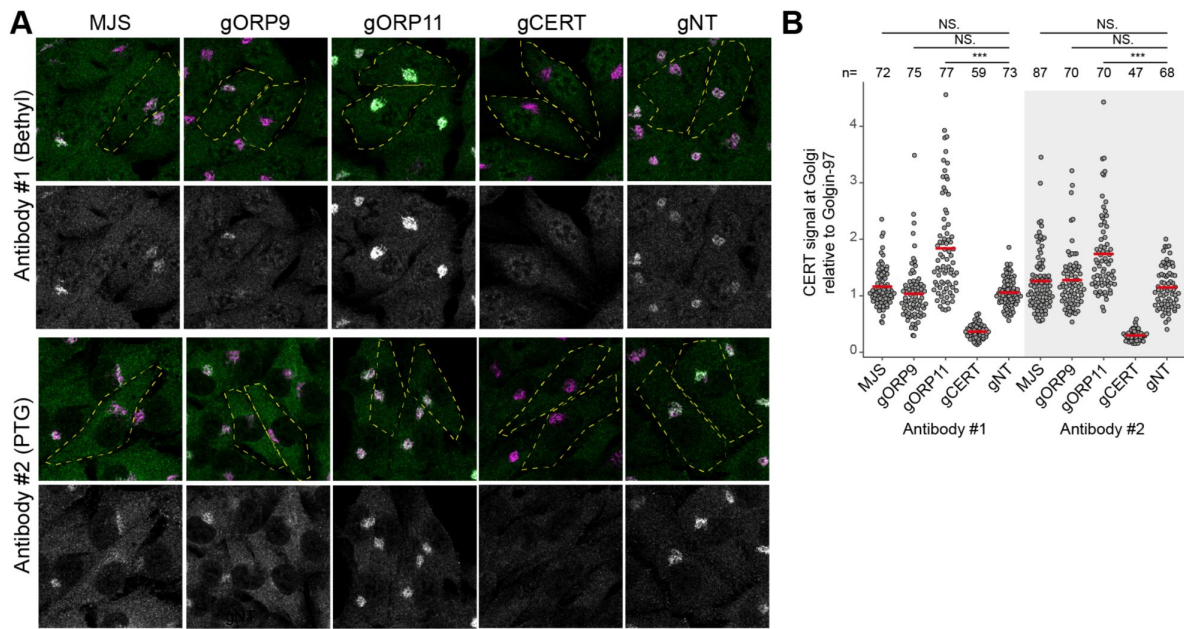
(A) Coomassie Blue staining of recombinant OSBP-related domains of ORP9 and ORP11. (B) ORP9 and ORP11 contain the critical residues for PS transfer.



Supplementary Figure 8

Loss of ORP9 or ORP11 does not affect sphingomyelin synthase levels.

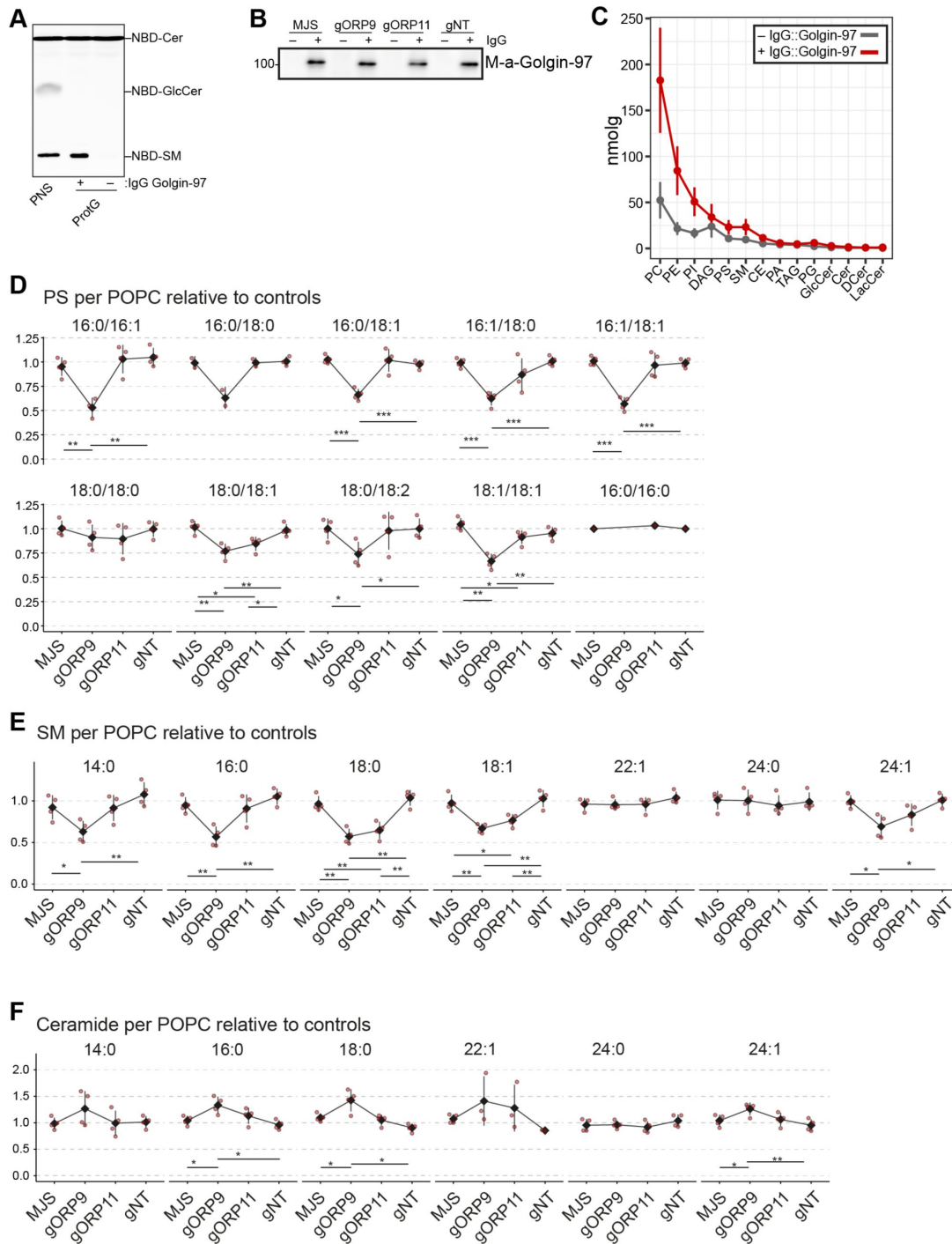
(A) Western blot analysis showing that the protein two human sphingomyelin synthases, SMS1 and SMS2, are not affected in ORP9 and ORP11 knockouts. (B) qRT-PCR showing that mRNA levels of SMS1 and SMS2 are not affected dramatically in knockout cells. Two primer sets per protein each was used (shown with roman numbers). Red lines correspond to mean values. (C) Thin-layer chromatography analysis visualizing the conversion of palmitic acid alkyne to sphingomyelin. To define the band corresponding to sphingomyelin, cells were treated with PDMP or with a cocktail of fumonisin B1 and myriocin prior to alkaline hydrolysis. (D) Golgi quantification of the DAG sensor, mCherry-C1ab, indicates reduced DAG levels in this organelle. Red lines correspond to mean from 3 experiments.



Supplementary Figure 9

CERT is not less present in the Golgi of ORP9 and ORP11 knockouts.

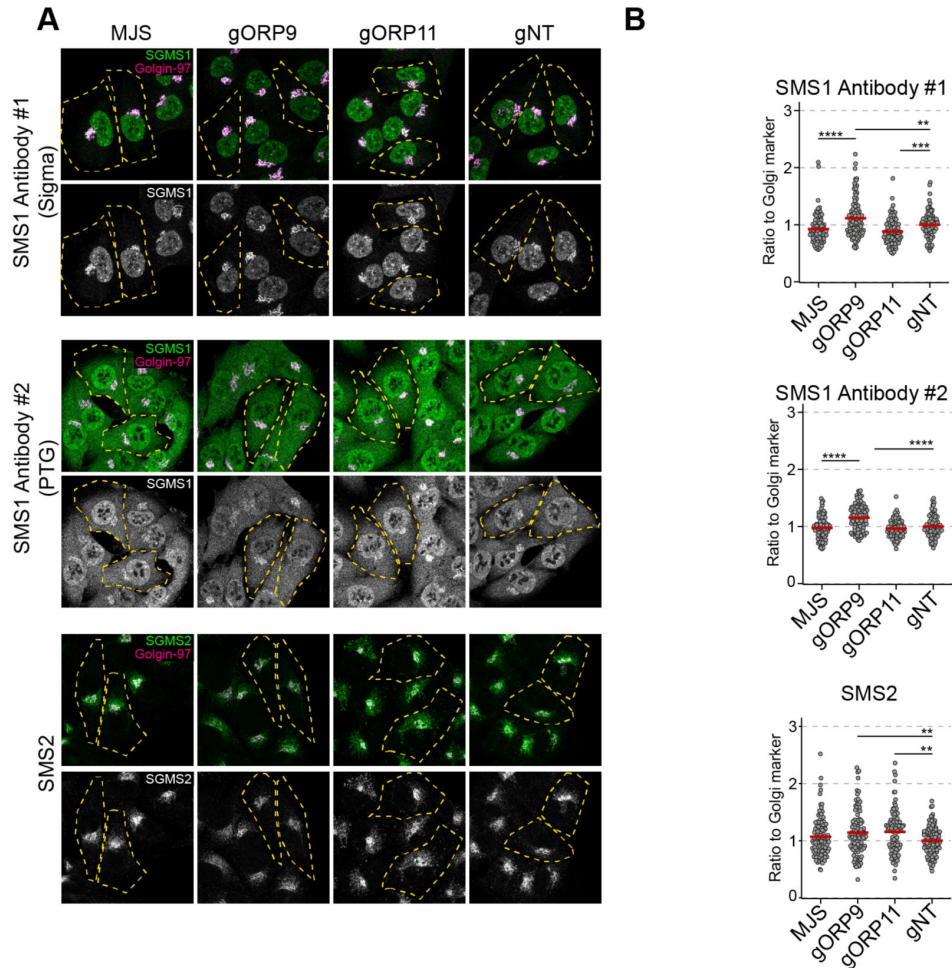
(A) Immunofluorescent staining of ORP9, ORP11 and CERT knockout cells using two antibodies against CERT. Note that antibodies fail to stain the Golgi in CERT knockouts. (B) Quantifications corresponding to panel A. Loss of ORP9 or ORP11 do not reduce CERT localization at the Golgi. Note that loss of ORP11 increases CERT localization at the Golgi, shown by two antibodies. Red lines correspond to mean from 3 experiments.



Supplementary Figure 10

Immunomagnetic isolation yields to intact Golgi membranes.

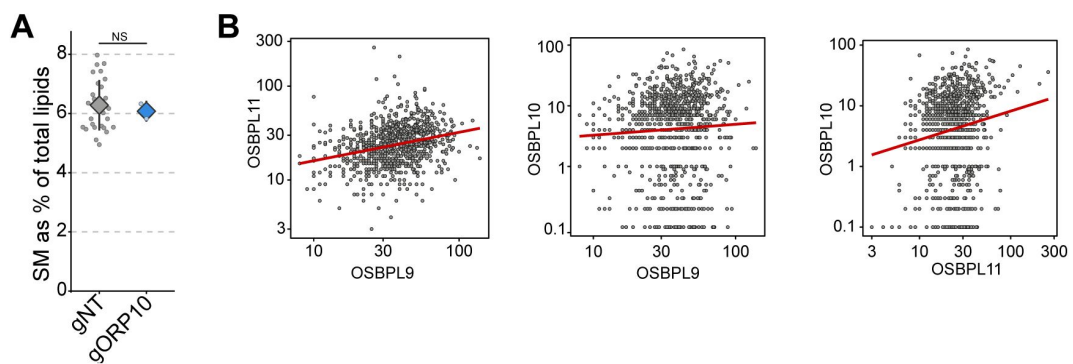
(A) Sphingomyelin synthase enzymatic activity assay performed on immunomagnetic Golgi isolates shows that the isolated membranes are intact and enzymatically active. Sphingomyelin synthases contain six transmembrane helices and require intact membrane for activity (Tafesse et al. 2006 "The Multigenic Sphingomyelin Synthase Family" J Biol Chem Volume 281, Issue 40). (B) Western blotting of immunomagnetic Golgi isolations from knockout cells using Golgin-97 antibody. (C) Amount of lipids isolated from samples in the absence or presence of the *trans* Golgi specific antibody Golgin-97. The plot is based on 16 data points obtained from n=4 experiments. Data points and error bars correspond to mean and standard deviations, respectively. (D) Distribution of PS species. (E) Distribution of sphingomyelin species. (F) Distribution of ceramide species.



Supplementary Figure 11

Golgi localization of sphingomyelin synthases is not reduced in ORP9 and ORP11 knockout cells.

(A) Immunofluorescence images showing localization of sphingomyelin synthases in ORP9 and ORP11 knockout cells. (B) Quantification of images corresponding to panel A. Note that the localization of SMS1 or SMS2 is not reduced in the knockout cells. An increased localization for SMS1 in the Golgi apparatus in ORP9 knockout cells is detected by two antibodies. Red lines correspond to mean from 3 experiments.



Supplementary Figure 12

ORP10 knockouts do not display sphingolipid imbalances.

(A) Lipidomics analysis of ORP10 knockouts do not reveal sphingolipid imbalances that are observed in ORP9 or ORP11 knockouts. (B) Expression analysis from Cancer Cell Line Encyclopedia shows that ORP9, ORP10 and ORP11 are not differentially expressed, but show a positive correlation.

References

1. van Meer G., de Kroon A. I. P. M (2011) **Lipid map of the mammalian cell** *J. Cell Sci* **124**:5–8
2. Wong L. H., Gatta A. T., Levine T. P (2019) **Lipid transfer proteins: the lipid commute via shuttles, bridges and tubes** *Nature Reviews Molecular Cell Biology* **20**:85–101
3. Chiapparino A., Maeda K., Turei D., Saez-Rodriguez J., Gavin A. C (2016) **The orchestra of lipid-transfer proteins at the crossroads between metabolism and signaling** *Prog. Lipid Res* **61**:30–39
4. Scorrano L., et al. (2019) **Coming together to define membrane contact sites** *Nat. Commun* **10**:1–11
5. Prinz W. A., Toulmay A., Balla T (2019) **The functional universe of membrane contact sites** *Nat. Rev. Mol. Cell Biol* **21**
6. Gatta A. T., et al. (2015) **A new family of StART domain proteins at membrane contact sites has a role in ER-PM sterol transport** *Elife* **4**:1–46
7. Sandhu J., et al. (2018) **Aster Proteins Facilitate Nonvesicular Plasma Membrane to ER Cholesterol Transport in Mammalian Cells** *Cell* **175**:514–529
8. Valverde D. P., et al. (2019) **ATG2 transports lipids to promote autophagosome biogenesis** *J. Cell Biol* **218**:1787–1798
9. Osawa T., et al. (2019) **Atg2 mediates direct lipid transfer between membranes for autophagosome formation** *Nat. Struct. Mol. Biol* **26**:281–288
10. Yeo H. K., et al. (2021) **Phospholipid transfer function of PTPIP51 at mitochondria-associated ER membranes** *EMBO Rep* **22**
11. Kumar N., et al. (2018) **VPS13A and VPS13C are lipid transport proteins differentially localized at ER contact sites** *J. Cell Biol* **217**:3625–3639
12. Castro I. G., et al. (2022) **Systematic analysis of membrane contact sites in *Saccharomyces cerevisiae* uncovers modulators of cellular lipid distribution** *Elife* **11**
13. Neuman S. D., Levine T. P., Bashirullah A (2022) **A novel superfamily of bridge-like lipid transfer proteins** *Trends Cell Biol* **32**:962–974
14. Holthuis J. C. M., Menon A. K (2014) **Lipid landscapes and pipelines in membrane homeostasis** *Nature* **510**:48–57
15. Hanada K., et al. (2003) **Molecular machinery for non-vesicular trafficking of ceramide** *Nature* **426**:803–809
16. Wong C. H., et al. (2023) **Genome-scale requirements for dynein-based trafficking revealed by a high-content arrayed CRISPR screen** *bioRxiv* <https://doi.org/10.1101/2023.03.01.530592>

17. Reza S., Ugorski M., Suchański J (2021) **Glucosylceramide and galactosylceramide, small glycosphingolipids with significant impact on health and disease** *Glycobiology* **31**:1416–1434
18. Nurmi H., et al. (2023) **Glycolipid transfer protein knockout disrupts vesicle trafficking to the plasma membrane** *J. Biol. Chem* **299**
19. Platt F. M (2014) **Sphingolipid lysosomal storage disorders** *Nature* **510**:68–75
20. Newton J., Milstien S., Spiegel S (2018) **Niemann-Pick type C disease: The atypical sphingolipidosis** *Adv. Biol. Regul* **70**:82–88
21. Sokoya T., et al. (2022) **Pathogenic variants of sphingomyelin synthase SMS2 disrupt lipid landscapes in the secretory pathway** *Elife* **11**
22. Deng Y., Rivera-Molina F. E., Toomre D. K., Burd C. G (2016) **Sphingomyelin is sorted at the trans Golgi network into a distinct class of secretory vesicle** *Proc. Natl. Acad. Sci. U. S. A* **113**:6677–6682
23. Kumagai K., Hanada K (2019) **Structure, functions and regulation of CERT, a lipid-transfer protein for the delivery of ceramide at the ER-Golgi membrane contact sites** *FEBS Lett* **593**:2366–2377
24. Zhou Y., et al. (2010) **OSBP-related protein 11 (ORP11) dimerizes with ORP9 and localizes at the Golgi- late endosome interface** *Exp. Cell Res* **316**:3304–3316
25. Neefjes J., Cabukusta B (2021) **What the VAP: The Expanded VAP Family of Proteins Interacting With FFAT and FFAT-Related Motifs for Interorganellar Contact** *Contact* **4**
26. Di Mattia T., et al. (2018) **Identification of MOSPD2, a novel scaffold for endoplasmic reticulum membrane contact sites** *EMBO Rep* **19**:1–22
27. Cabukusta B., et al. (2020) **Human VAPome Analysis Reveals MOSPD1 and MOSPD3 as Membrane Contact Site Proteins Interacting with FFAT-Related FFNT Motifs** *Cell Rep* **33**
28. Levine T. P., Munro S (1998) **The pleckstrin homology domain of oxysterol-binding protein recognises a determinant specific to Golgi membranes** *Curr. Biol* **8**:729–739
29. Levine T. P., Munro S (2002) **Targeting of Golgi-specific pleckstrin homology domains involves both PtdIns 4-kinase-dependent and -independent components** *Curr. Biol* **12**:695–704
30. Wang H., et al. (2019) **ORP2 Delivers Cholesterol to the Plasma Membrane in Exchange for Phosphatidylinositol 4, 5-Bisphosphate (PI(4,5)P 2)** *Mol. Cell* **73**:458–473
31. Mesmin B., et al. (2013) **A four-step cycle driven by PI(4)P hydrolysis directs sterol/PI(4)P exchange by the ER-Golgi Tether OSBP** *Cell* **155**:830–843
32. de Saint-Jean M., et al. (2011) **Osh4p exchanges sterols for phosphatidylinositol 4-phosphate between lipid bilayers** *J. Cell Biol* **195**:965–978
33. Maeda K., et al. (2013) **Interactome map uncovers phosphatidylserine transport by oxysterol-binding proteins** *Nature* **501**:257–261

34. Tan J. X., Finkel T (2022) **A phosphoinositide signalling pathway mediates rapid lysosomal repair** *Nature* **609**:815–821
35. Kawasaki A., et al. (2021) **PI4P/PS countertransport by ORP10 at ER-endosome membrane contact sites regulates endosome fission** *J. Cell Biol* **221**
36. He R., et al. (2023) **ORP9 and ORP10 form a heterocomplex to transfer phosphatidylinositol 4-phosphate at ER-TGN contact sites** *Cell. Mol. Life Sci* **80**
37. Ikhlef S., et al. (2021) **Functional analyses of phosphatidylserine/PI(4)P exchangers with diverse lipid species and membrane contexts reveal unanticipated rules on lipid transfer** *BMC Biol* **19**
38. Chung J., et al. (2015) **PI4P/phosphatidylserine countertransport at ORP5- and ORP8-mediated ER - Plasma membrane contacts** *Science (80-.)* **349**:428–432
39. Von Filseck J. M., et al. (2015) **Phosphatidylserine transport by ORP/Osh proteins is driven by phosphatidylinositol 4-phosphate** *Science* **349**:432–436
40. Posor Y., Jang W., Haucke V (2022) **Phosphoinositides as membrane organizers** *Nat. Rev. Mol. Cell Biol* **23**:797–816
41. Yeung T., et al. (2008) **Membrane phosphatidylserine regulates surface charge and protein localization** *Science* **319**:210–213
42. Moorhead A. M., Jung J. Y., Smirnov A., Kaufer S., Scidmore M. A (2010) **Multiple host proteins that function in phosphatidylinositol-4-phosphate metabolism are recruited to the chlamydial inclusion** *Infect. Immun* **78**:1990–2007
43. Kol M., et al. (2017) **Switching head group selectivity in mammalian sphingolipid biosynthesis by active- site-engineering of sphingomyelin synthases** *J. Lipid Res* **58**:962–973
44. Tafesse F. G., Ternes P., Holthuis J. C. M (2006) **The multigenic sphingomyelin synthase family** *J. Biol. Chem* **281**:29421–29425
45. Capasso S., et al. (2017) **Sphingolipid metabolic flow controls phosphoinositide turnover at the trans-Golgi network** *EMBO J* **36**:1736–1754
46. Peretti D., Dahan N., Shimoni E., Hirschberg K., Lev S (2008) **Coordinated lipid transfer between the endoplasmic reticulum and the Golgi complex requires the VAP proteins and is essential for Golgi- mediated transport** *Mol. Biol. Cell* **19**:3871–3884
47. Horibata Y., Sugimoto H (2010) **StarD7 mediates the intracellular trafficking of phosphatidylcholine to mitochondria** *J. Biol. Chem* **285**:7358–7365
48. Saita S., et al. (2018) **PARG partitions the lipid transfer protein STARD7 between the cytosol and mitochondria** *EMBO J* **37**:1–18
49. Horibata Y., et al. (2016) **StarD7 protein deficiency adversely affects the phosphatidylcholine composition, respiratory activity, and cristae structure of mitochondria** *J. Biol. Chem* **291**:24880–24891
50. Venditti R., et al. (2019) **Molecular determinants of ER-Golgi contacts identified through a new FRET-FLIM system** *J. Cell Biol* **218**:1055–1065

51. Ridgway N. D., Dawson P. A., Ho Y. K., Brown M. S., Goldstein J. L (1992) **Translocation of oxysterol binding protein to Golgi apparatus triggered by ligand binding** *J. Cell Biol* **116**:307–319
52. de la Mora E., et al. (2021) **Nanoscale architecture of a VAP-A-OSBP tethering complex at membrane contact sites** *Nat. Commun* **12**
53. Gehin C., et al. (2023) **CERT1 mutations perturb human development by disrupting sphingolipid homeostasis** *J. Clin. Invest* **133**
54. Peretti D., Kim S., Tufi R., Lev S (2020) **Lipid Transfer Proteins and Membrane Contact Sites in Human Cancer** *Front. Cell Dev. Biol* **7**:1–14
55. Mizuike A., Hanada K (2024) **DGARM/C10orf76/ARMH3 for Ceramide Transfer Zone at the Endoplasmic Reticulum–Distal Golgi Contacts** *Contact* **7**
56. Cockcroft S., Lev S (2020) **Mammalian PITPs at the Golgi and ER-Golgi Membrane Contact Sites** *Contact* **3**
57. Radulovic M., et al. (2022) **Cholesterol transfer via endoplasmic reticulum contacts mediates lysosome damage repair** *EMBO J* **41**
58. Vacaru A. M., et al. (2009) **Sphingomyelin synthase-related protein SMSr controls ceramide homeostasis in the ER** *J. Cell Biol* **185**:1013–1027
59. Mesmin B., et al. (2017) **Sterol transfer, PI 4P consumption, and control of membrane lipid order by endogenous OSBP** *EMBO J* **36**:3156–3174
60. Doench J. G., et al. (2016) **Optimized sgRNA design to maximize activity and minimize off-target effects of CRISPR-Cas9** *Nat. Biotechnol* **34**:184–191
61. Sanjana N. E., Shalem O., Zhang F (2014) **Improved vectors and genome-wide libraries for CRISPR screening** *Nat. Methods* **11**:783–784
62. Wijdeven R. H., et al. (2022) **CRISPR Activation Screening Identifies VGLL3-TEAD1-RUNX1/3 as a Transcriptional Complex for PD-L1 Expression** *J. Immunol* <https://doi.org/10.4049/JIMMUNOL.2100917>
63. Ghorasaini M., et al. (2021) **Cross-Laboratory Standardization of Preclinical Lipidomics Using Differential Mobility Spectrometry and Multiple Reaction Monitoring** *Anal. Chem* **93**:16369–16378
64. Su B., et al. (2021) **A DMS Shotgun Lipidomics Workflow Application to Facilitate High-Throughput, Comprehensive Lipidomics** *J. Am. Soc. Mass Spectrom* **32**:2655–2663
65. Faas F. G. A., et al. (2012) **Virtual nanoscopy: generation of ultra-large high resolution electron microscopy maps** *J. Cell Biol* **198**:457–469
66. Jumper J., et al. (2021) **Highly accurate protein structure prediction with AlphaFold** *Nature* **596**:583–589
67. Mirdita M., et al. (2022) **ColabFold: making protein folding accessible to all** *Nat. Methods* **19**:679–682

68. Evans R., et al. (2022) **Protein complex prediction with AlphaFold-Multimer** *bioRxiv* <https://doi.org/10.1101/2021.10.04.463034>
69. Barretina J., et al. (2012) **The Cancer Cell Line Encyclopedia enables predictive modelling of anticancer drug sensitivity** *Nature* **483**:603–607
70. Zewe J. P., Wills R. C., Sangappa S., Goulden B. D., Hammond G. R (2018) **SAC1 degrades its lipid substrate PtdIns4P in the endoplasmic reticulum to maintain a steep chemical gradient with donor membranes** *Elife* **7**

Editors

Reviewing Editor

Felix Campelo

Institute of Photonic Sciences, Barcelona, Spain

Senior Editor

Amy Andreotti

Iowa State University, Ames, United States of America

Reviewer #1 (Public Review):

Summary:

In this well-designed study, the authors of the manuscript have analyzed the impact of individually silencing 90 lipid transfer proteins on the overall lipid composition of a specific cell type. They confirmed some of the evidence obtained by their own and other research groups in the past, and additionally, they identified an unreported role for ORP9-ORP11 in sphingomyelin production at the trans-Golgi. As they delved into the nature of this effect, the authors discovered that ORP9 and ORP11 form a dimer through a helical region positioned between their PH and ORD domains.

Strengths:

This well-designed study presents compelling new evidence regarding the role of lipid transfer proteins in controlling lipid metabolism. The discovery of ORP9 and ORP11's involvement in sphingolipid metabolism invites further investigation into the impact of the membrane environment on sphingomyelin synthase activity.

Weaknesses:

There are a couple of weaknesses evident in this manuscript. Firstly, there's a lack of mechanistic understanding regarding the regulatory role of ORP9-11 in sphingomyelin synthase activity. Secondly, the broader role of hetero-dimerization of LTPs at ER-Golgi membrane contact sites is not thoroughly addressed. The emerging theme of LTP dimerization through coiled domains has been reported for proteins such as CERT, OSBP, ORP9, and ORP10. However, the specific ways in which these LTPs hetero and/or homo-dimerize and how this impacts lipid fluxes at ER-Golgi membrane contact sites remain to be fully understood.

Regardless of the unresolved points mentioned above, this manuscript presents a valuable conceptual advancement in the study of the impact of lipid transfer on overall lipid metabolism. Moreover, it encourages further exploration of the interplay among LTP actions across various cellular organelles.

Reviewer #2 (Public Review):

Summary:

The authors set out to determine which lipid transfer proteins impact the lipids of Golgi apparatus, and they identified a reasonable number of "hits" where the lack of one lipid transfer protein affected a particular Golgi lipid or class of lipids. They then carried out something close to a "proof of concept" for one lipid (sphingomyelin) and two closely related lipid transfer proteins (ORP9/ORP11). They looked into that example in great detail and found a previous unknown relationship between the level of phosphatidylserine in the Golgi (presumably trans-Golgi, trans-Golgi Network) and function of the sphingomyelin synthase enzyme. This was all convincingly done - results support their conclusions - showing that the authors achieved their aims.

Impact:

There are likely to be 2 types of impact:

(i) cell biology: sphingomyelin synthase, ORP9/11 will be studied in future in more informed ways to understand (a) the role of different Golgi lipids - this work opens that out and produces a to more questions than answers (b) the role of different ORPs: what distinguishes ORP11 from its paralogy ORP10?

(ii) molecular biochemistry: combining knockdown miniscreen with organelle lipidomics must be time-consuming, but here it is shown to be quite a powerful way to discover new aspects of lipid-based regulation of protein function. This will be useful to others as an example, and if this kind of workflow could be automated, then the possible power of the method could be widely applied.

Strengths:

Nicely controlled data;

Wide-ranging lipidomics dataset with repeats and SDs - all data easily viewed.

Simple take home message that PS traffic to the TGN by ORP9/11 is required for some aspect of SMS1 function.

Weaknesses:

Model and Discussion:

Despite the authors saying that this has been addressed in their rebuttal, I still struggle to find any ideas about the aspect of SMS1 function that is being affected.

As I mentioned before, even if no further experiments were carried out the authors could discuss possibilities. one might speculate what the PS is being used for. For example, is it a co-factor for integral membrane proteins, such as flippases? Is it a co-factor for peripheral membrane proteins, such as yet more LTPs? The model could include the work of Peretti et al (2008), which linked Nir2 activity exchanging PI:PA (Yadav et al, 2015) to the eventual function of CERT. Could the PS have a role in removing/reducing DAG produced by CERT?

<https://doi.org/10.7554/eLife.91345.2.sa1>

Author response:

The following is the authors' response to the original reviews.

Reviewer #1 (Recommendations For The Authors):

The authors should possibly discuss more the other cases when LTPs of the same type of ORP9 and ORP10 have been found to dimerise. They should definitely cite and discuss the evidence reported in February this year in CMLS (see <https://link.springer.com/article/10.1007/s00018-023-04728-5>). In this paper, authors reported very similar findings as those the authors have in Figures 3, 4, S6, S7, and S8. Specifically, in this CMLS paper the authors find that ORP9 and ORP10 (not ORP11) interact through a central helical region and that ORP9 localises ORP10 to the ER-Golgi MCSs by providing ORP10 with a binding site for VAPs, where the heterodimer mediates the exchange of PtdIns(4)P for PtdSer.

We thank the reviewer for their recommendations. The mentioned paper has simply gone unnoticed by us and is now referred in the revised manuscript. Various other papers reporting on LTP dimerizations are already cited in our manuscript: ORP9-ORP10 dimerization (Kawasaki et al. 2022), ORP9-ORP11 dimerization (Zhou et al. 2010), and ORP9-ORP10/11 dimerization (Tan and Finkel 2022). Revised manuscript now discusses the dimerization of CERT and OSBP while citing Gehin et al. 2023, Ridgway et al. 1992 and de la Mora et al. 2021.

Reviewer #2 (Recommendations For The Authors):

Model and Discussion:

Give an idea about the aspect of SMS1 function that is being affected. Even if no further experiments were carried out, the authors could discuss possibilities. One might speculate what the PS is being used for. For example, is it a co-factor for integral membrane proteins, such as flippases? Is it a co-factor for peripheral membrane proteins, such as yet more LTPs? The model could include the work of Peretti et al (2008), which linked Nir2 activity exchanging PI:PA (Yadav et al, 2015) to the eventual function of CERT. Could the PS have a role in removing/reducing DAG produced by CERT?

We thank the reviewer for their recommendations. The same recommendations were also scripted in the public review, which we believe we answered sufficiently.

Other, Minor:

Make clear that there is no sterol readout (Fig 1C)

We would like to point out that Figure 1C has a sterol readout as CE refers to cholesterol esters.

PH domains of ORP9 and ORP11 localized only partially to the Golgi, unlike the PH domains of OSBP and CERT" (line 154). Say here where the non-Golgi ORP9 and ORP11 PH domain pool is - presumably in the cytoplasm.

We thank the reviewer for their suggestion and rephrase the sentence accordingly.

Fig 7H-J: histograms not lines as these are separate unlinked categories

We thank the reviewer for their suggestion. However, we think the original figure represent our findings in the best possible way. Our analysis regarding individual lipid species is also

included in Supplementary figure 10.

Reviewer #3 (Recommendations For The Authors):

(1) At the end of the intro, in summarizing their findings, the authors state (p3, lines 48-49) "These findings highlight how phospholipid and sphingolipid gradients along the secretory pathway are linked at ER-Golgi membrane contact sites." This should instead read "These findings highlight THAT phospholipid and sphingolipid gradients along the secretory pathway are linked at ER-Golgi membrane contact sites."

We thank the reviewer for their suggestion and change the sentence accordingly.

(2) As noted in the public section, to show that ORP9/11 do indeed exchange lipids, an in vitro experiment demonstrating that ORP11 can transfer PI4P is essential. Ideally, it would be best to examine PS AND PI4P transfer by ORP9 AND 11 separately AND then by the ORP9/11 heterodimer. This could lend insights as to the function of the heterodimer. The He et al et Yu paper should provide guidelines for this. Why have the heterodimers?

We believe we addressed this point by showing the lipid transfer ability of the ORP9-ORP11 dimer. These findings are now part of the revised manuscript.

(3) It would be interesting to discuss the roles of ORP9/ORP11 versus ORP9/ORP10... they seem so analogous, although this is at the discretion of the authors.

We thank the reviewer for their suggestion. Since the difference between ORP9-ORP10 and ORP9-ORP11 dimers was also raised by other reviewers, we decided to include this discussion in the manuscript. A section based on our answer to Reviewer #2 in Public Review is now part of the Discussions.

(4) The authors used a melanoma cell line in their screens (p3, line 59). Could they explain why they used this cell line versus others?

We chose MelJuSo cell for various reasons. Mainly, MelJuSo are diploid, which eases generating knockouts in a screening setup compared to other polyploid cancer cell lines (e.g. HeLa). Furthermore, our CRISPR/Cas9 screening protocols are optimized for these cell lines.

<https://doi.org/10.7554/eLife.91345.2.sa0>